inorganics

MDPI

Article

Isomeric 4,2′:6′,4″- and 3,2′:6′,3″-Terpyridines with Isomeric 4′-Trifluoromethylphenyl Substituents: Effects on the Assembly of Coordination Polymers with [Cu(hfacac)$_2$] (Hhfacac = Hexafluoropentane-2,4-dione)

Giacomo Manfroni, Simona S. Capomolla, Alessandro Prescimone, Edwin C. Constable and Catherine E. Housecroft *

Department of Chemistry, University of Basel, BPR 1096, Mattenstrasse 24a, CH-4058 Basel, Switzerland; giacomo.manfroni@unibas.ch (G.M.); simona.capomolla@unibas.ch (S.S.C.); alessandro.prescimone@unibas.ch (A.P.); edwin.constable@unibas.ch (E.C.C.)

* Correspondence: catherine.housecroft@unibas.ch

Abstract: The isomers 4′-(4-(trifluoromethyl)phenyl)-4,2′:6′,4″-terpyridine (**1**), 4′-(3-(trifluoromethyl)phenyl)-4,2′:6′,4″-terpyridine (**2**), 4′-(4-(trifluoromethyl)phenyl)-3,2′:6′,3″-terpyridine (**3**), and 4′-(3-(trifluoromethyl)phenyl)-3,2′:6′,3″-terpyridine (**4**) have been prepared and characterized. The single crystal structures of **1** and **2** were determined. The 1D-polymers $[Cu_2(hfacac)_4(\mathbf{1})_2]_n \cdot 2n C_6H_4Cl_2$ (Hhfacac = 1,1,1,5,5,5-hexafluoropentane-2,4-dione), $[Cu(hfacac)_2(\mathbf{2})]_n \cdot 2n C_6H_5Me$, $[Cu_2(hfacac)_4(\mathbf{3})_2]_n \cdot n C_6H_4Cl_2$, $[Cu_2(hfacac)_4(\mathbf{3})_2]_n \cdot n C_6H_5Cl$, and $[Cu(hfacac)_2(\mathbf{4})]_n \cdot n C_6H_5Cl$ have been formed by reactions of **1**, **2**, **3** and **4** with $[Cu(hfacac)_2] \cdot H_2O$ under conditions of crystal growth by layering and four of these coordination polymers have been formed on a preparative scale. $[Cu_2(hfacac)_4(\mathbf{1})_2]_n \cdot 2n C_6H_4Cl_2$ and $[Cu(hfacac)_2(\mathbf{2})]_n \cdot 2n C_6H_5Me$ are zig-zag chains and the different substitution position of the CF_3 group in **1** and **2** does not affect this motif. Packing of the polymer chains is governed mainly by C–F...F–C contacts, and there are no inter-polymer π-stacking interactions. The conformation of the 3,2′:6′,3″-tpy unit in $[Cu_2(hfacac)_4(\mathbf{3})_2]_n \cdot n C_6H_4Cl_2$ and $[Cu(hfacac)_2(\mathbf{4})]_n \cdot n C_6H_5Cl$ differs, leading to different structural motifs in the 1D-polymer backbones. In $[Cu(hfacac)_2(\mathbf{4})]_n \cdot n C_6H_5Cl$, the peripheral 3-$CF_3C_6H_4$ unit is accommodated in a pocket between two {Cu(hfacac)$_2$} units and engages in four C–H_{phenyl}...F–C_{hfacac} contacts which lock the phenylpyridine unit in a near planar conformation. In $[Cu_2(hfacac)_4(\mathbf{3})_2]_n \cdot n C_6H_4Cl_2$ and $[Cu(hfacac)_2(\mathbf{4})]_n \cdot n C_6H_5Cl$, π-stacking interactions between 4′-trifluoromethylphenyl-3,2′:6′,3″-tpy domains are key packing interactions, and this contrasts with the packing of polymers incorporating **1** and **2**. We use powder X-ray diffraction to demonstrate that the assemblies of the coordination polymers are reproducible, and that a switch from a 4,2′:6′,4″- to 3,2′:6′,3″-tpy metal-binding unit is accompanied by a change from dominant C–F...F–C and C–F...H–C contacts to π-stacking of arene domains between ligands **3** or **4**.

Keywords: copper; 4,2′:6′,4″-terpyridine; 3,2′:6′,3″-terpyridine; coordination polymer; isomers

Citation: Manfroni, G.; Capomolla, S.S.; Prescimone, A.; Constable, E.C.; Housecroft, C.E. Isomeric 4,2′:6′,4″- and 3,2′:6′,3″-Terpyridines with Isomeric 4′-Trifluoromethylphenyl Substituents: Effects on the Assembly of Coordination Polymers with [Cu(hfacac)$_2$] (Hhfacac = Hexafluoropentane-2,4-dione). *Inorganics* **2021**, *9*, 54. https://doi.org/10.3390/inorganics9070054

Academic Editor: Duncan H. Gregory

Received: 1 June 2021
Accepted: 7 July 2021
Published: 10 July 2021

1. Introduction

The coordination chemistry of the 4,2′:6′,4″- and 3,2′:6′,3″-isomers of terpyridine (4,2′:6′,4″-tpy and 3,2′:6′,3″-tpy, Scheme 1) has attracted significant attention in the last decade because the vectorial properties of these isomers of tpy are suited to the assembly of coordination polymers and networks [1–6]. As Scheme 1 illustrates, 4,2′:6′,4″-tpy and 3,2′:6′,3″-tpy only coordinate through the outer pyridine donors, leaving the central nitrogen atom unbound. This provides a strategy for the design of coordination assemblies in which the surfaces of the solvent-accessible channels contain sites of Lewis basicity potentially leading to small molecule recognition through, e.g., C–H...$N_{pyridine}$ hydrogen bond formation [5], and sensing applications [5–9]. Moreover, 3,2′:6′,3″-tpy exhibits greater

conformational flexibility than 4,2′:6′,4″-tpy (Scheme 1), leading to greater variation (or less predictability) in network assembly [4].

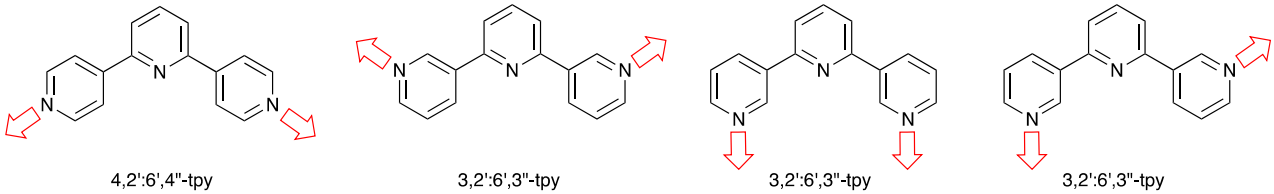

Scheme 1. 4,2′:6′,4″- and 3,2′:6′,3″-Terpyridines typically coordinate through the outer pyridine donors rendering them as divergent linkers. The three limiting, planar conformations of 3,2′:6′,3″-tpy are shown.

Although a wide range of 1D-, 2D- and 3D-assemblies incorporating 4,2′:6′,4″-tpy metal-binding domains is known, those with 3,2′:6′,3″-tpy ligands are less well explored [1–5]. Coordination assemblies involving Cu(II) or Cu(I) fall into several categories. A well-represented group involves $\{Cu_2(\mu\text{-}OAc)_4\}$ paddle-wheel units connected into 1D-polymer chains by ditopic 4,2′:6′,4″-tpy or 3,2′:6′,3″-tpy linkers [10–16]. A number of architectures feature $\{Cu^{II}{}_2Cl_4\}$ [17] and $\{Cu^{I}{}_2I_2\}$ nodes [18–20], or $\{Cu^{I}{}_n(CN)_n\}$ building blocks [21–24]. We note, however, that when 1-(3,2′:6′,3″-terpyridin-4′-yl)ferrocene reacts with $CuCl_2$, $\{Cu^{II}{}_2Cl_4\}$ building blocks interconnect 3,2′:6′,3″-tpy units in conformation **C** (Scheme 1) to give a discrete molecular complex [25]. Introducing carboxylic acid substituents into the 4,2′:6′,4″- or 3,2′:6′,3″-tpy units is a strategy for increasing the donor capacity of the ligand, thereby increasing the dimensionality of the assembly. Typically, the carboxylic acid is deprotonated and the $CO_2{}^-$ group supplements the *N*,*N*′-donor set of tpy. Examples include 4′-carboxylato-4,2′:6′,4′′-terpyridine [26], 4′-(4-carboxylatophenyl)-4,2′:6′,4′′-terpyridine [22,27], 3,5-dicyano-4′-(4-carboxylatophenyl)-4,2′:6′,4″-terpyridine [28], and 4′-(4-(3,5-dicarboxylatophenoxy)phenyl)-4,2′:6′,4′′-terpyridine [29]. Assemblies combining Cu(II) and sulfonic acid-functionalized tpy ligands are less well represented [30]. In the case of 4′-(4-hydroxyphenyl)-4,2′:6′,4′′-terpyridine (4′-(HOC_6H_4)-4,2′:6′,4′′-tpy), the ligand coordinates only through the 4,2′:6′,4″-tpy unit in the 2D-networks $[\{Cu(OH_2)(4'\text{-}(HOC_6H_4)\text{-}4,2':6',4''\text{-}tpy)_2Cl\}_n][NO_3]_n$ and $[\{Cu(OH_2)_2(4'\text{-}(HOC_6H_4)\text{-}4,2':6',4''\text{-}tpy)_2\}_n][NO_3]_{2n}$ [31]. 3-Dimensional architectures directed by Cu(II) nodes in which the 4,2′:6′,4′′-tpy ligands are merely linkers are exemplified by the chiral $[\{Cu_2(DMSO)_3(4'\text{-}(MeOC_6H_4)\text{-}4,2':6',4''\text{-}tpy)_4\}_n][BF_4]_{4n}$ (4′-($MeOC_6H_4$)-4,2′:6′,4′′-tpy = 4′-(4-methoxyphenyl)-4,2′:6′,4′′-terpyridine) [32]. A further way of increasing dimensionality of an assembly is to introduce a 4′-pyridinyl (usually 4′-pyridin-4-yl) substituents into the tpy metal-binding domain. Zaworotko and coworkers have reported a beautiful series of 3D-networks featuring 8-connected $[Cu_2(py\text{-}4,2':6',4''\text{-}tpy)_8(\mu\text{-}MF_6)]^{2+}$ building blocks in which py-4,2′:6′,4′′-tpy is 4′-(pyridin-4-yl)-4,2′:6′,4′′-terpyridine, and M = Si, Ge, Sn, Ti or Zr [33].

Both the $\{Cu(acac)_2\}$ and $\{Cu(hfacac)_2\}$ units (Hacac = pentane-2,4-dione, Hhfacac = 1,1,1,5,5,5-hexafluoropentane-2,4-dione) are ubiquitous in coordination chemistry, although it is interesting that the latter is far better represented in the Cambridge Structural Database (CSD) [34] than the former. A search of the CSD, version 2020.3.1 [35] using ConQuest version 2020.3.1 [35] revealed 1039 hits for compounds containing a $\{Cu(hfacac)_2\}$ unit compared to 172 containing $\{Cu(acac)_2\}$; of these 172 hits, 62 are different determinations of polymorphs of the structure of $[Cu(acac)_2]$ (CSD refcode ACACCU). One reason for the dominance of $[hfacac]^-$ containing compounds may be that the presence of the CF_3 substituents improves the solubility of the Cu(II) salt in a wider range of solvents with respect to $[Cu(acac)_2]$. Although coordination polymers containing $\{Cu(hfacac)_2\}$ nodes are well established (557 hits in the CSD version 2020.3.1), examples incorporating divergent terpyridine ligands are rare. Moreno and coworkers described the syntheses and structural characterization of $[Cu(hfacac)_2(L_1)]_n$, $[Cu(hfacac)_2(L_2)]_n{\cdot}n CHCl_3$, $[Cu(hfacac)_2(L_3)]_n{\cdot}n CHCl_3$, and $[Cu(hfacac)_2(L_4)]_n$ (L_1–L_4 are defined in Scheme 2) [36]. All four compounds are

1D-coordination polymers with 4,2′:6′,4″- or 3,2′:6′,3″-tpy domains linking octahedral Cu(II) centers. However, whereas $[Cu(hfacac)_2(L_1)]_n$ and $[Cu(hfacac)_2(L_3)]_n \cdot CHCl_3$ contain a *cis*-arrangement of pyridine *N*-donors, the latter are in a *trans*-arrangement in $[Cu(hfacac)_2(L_2)]_n \cdot CHCl_3$ and $[Cu(hfacac)_2(L_4)]_n$. In $[Cu(hfacac)_2(L_3)]_n \cdot CHCl_3$, the 3,2′:6′,3″-tpy unit adopts conformation **A** shown in Scheme 1. Moreno has also reported that the reaction of L_1 with $[Cu(ttfacac)_2]$ (Httfacac = 4,4,4-trifluoro-1-(thiophen-2-yl)butane-1,3-dione) yielded the discrete, trinuclear complex $[Cu_3(ttfacac)_6(L_1)_2]$ [37]. Other relevant 1D-coordination polymers containing octahedral $\{Cu(hfacac)_2(N_{py})_2\}$ building blocks include $[Cu(hfacac)_2(4,4'\text{-bpy})]_n$ (4,4′-bpy = 4,4′-bipyridine) [38] and $[Cu(hfacac)_2(dpss)]_n$ (dpss = di(pyridin-2-yl disulfide) [39] in which the N_{py} donors are *trans*, and $[Cu(hfacac)_2(bpyb)]_n$ (bpyb = 1,4-bis(pyridin-2-yl)buta-1,3-diyne in which the N_{py} donors are mutually *cis* [39]. A combination of 1,3,5-tris(pyridin-4-ylethynyl)benzene (L_5, Scheme 2) with $[Cu(hfacac)_2]$ gives a 2D-network directed by the 3-connecting L_5 ligand; *trans*-$\{Cu(hfacac)_2(N_{py})_2\}$ units are present [40].

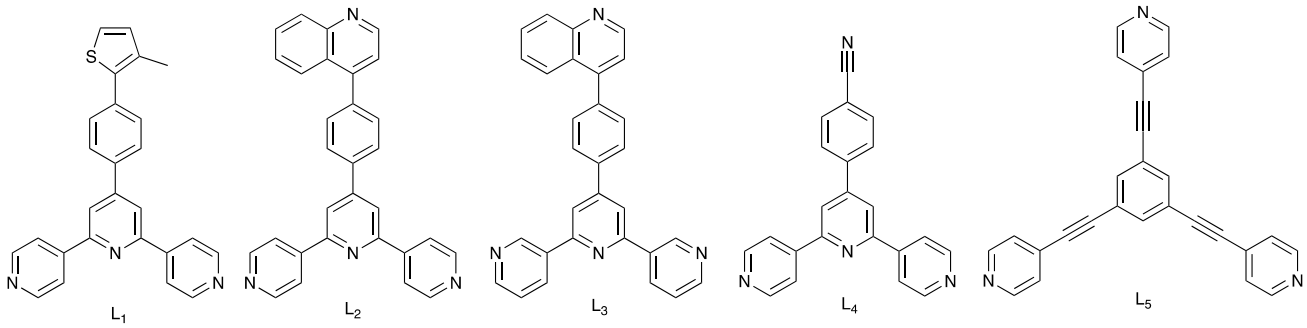

Scheme 2. The structures of ligands L_1, L_2, L_3, L_4 [36] and L_5 [40].

In order to complement both our own investigations of the coordination chemistry of 4,2′:6′,4″-tpy and 3,2′:6′,3″-tpy ligands and copper(II) salts [11–16], and the structural diversity of the known coordination polymers featuring $\{Cu(hfacac)_2\}$ nodes, we decided to explore the assemblies formed between $[Cu(hfacac)_2]$ and ligands **1–4** shown in Scheme 3. The ligand series was selected to combine isomers of the tpy metal-binding domain with isomers of the 4′-trifluoromethylphenyl substituent. The trifluoromethyl substituents were incorporated to give a complementarity to the $[hfacac]^-$ ligands, and potentially introduce additional supramolecular packing interactions within the lattice. The availability of the different trifluoromethylphenyl isomers as substituents allows the subtlety of the supramolecular interactions to be probed.

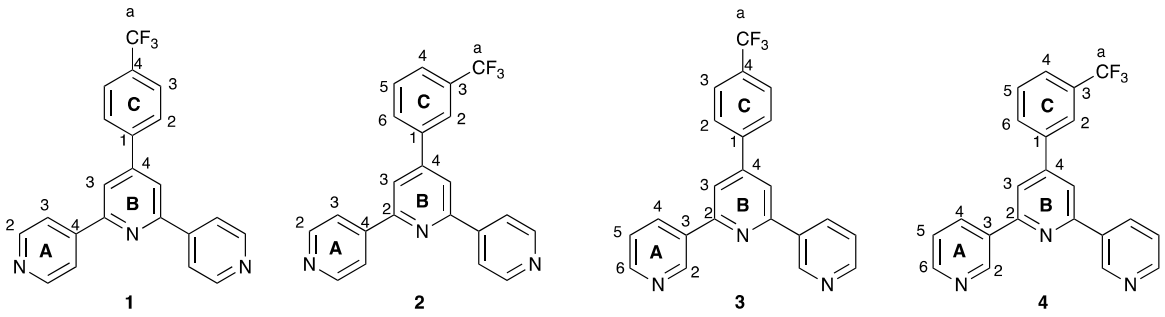

Scheme 3. Structures of ligands **1–4** with the numbering system used for NMR spectroscopic assignments.

2. Results and Discussion

*2.1. Syntheses and Characterization of Ligands **1**–**4***

Compounds **1**–**4** were prepared using the one-pot strategy of Wang and Hanan [41], (Scheme 4 for **1**). After purification, compounds **1**–**4** were isolated as colorless, microcrystalline solids in yields of between 31.3 and 49.3%. The four compounds are isomers and in the MALDI-TOF mass spectrum of each, the base peak corresponded to the $[M+H]^+$ ion (Figures S1–S4 in the Supporting Material). For **3** and **4**, which contain the 3,2′:6′,3″-tpy unit, the isotope pattern is as expected (Figures S3 and S4). However, for the derivatives of 4,2′:6′,4″-tpy (compounds **1** and **2**), the relative intensities of the peaks at *m/z* 378.1 and 379.1 (Figures S1 and S2) are consistent with both $[M+H]^+$ and $[M+2H]^{2+}$ ions. This is consistent with the greater basicity of 4,2′:6′,4″-tpy versus 3,2′:6′,3″-tpy. To support this, we considered the model compounds 3-phenylpyridine (3-Phpy) and 4-phenylpyridine (4-Phpy). The pK_a values of the conjugate acids $[H(4\text{-Phpy})]^+$ and $[H(3\text{-Phpy})]^+$ are 5.38 and 4.81, respectively [42], confirming that $[H(3\text{-Phpy})]^+$ is a stronger acid than $[H(4\text{-Phpy})]^+$ and, therefore, 4-Phpy is a stronger base then 3-Phpy. The solid-state IR spectra of **1**–**4** are shown in Figures S5–S8, and exhibit similar fingerprint regions. The absorption spectra of MeCN solutions of the terpyridine ligands are all similar (Figure S9) and the absorptions at λ_{max} = 248–250 nm and λ_{max} = 294–306 nm (see Sections 3.2–3.5) are assigned to $\pi^* \leftarrow \pi$ transitions.

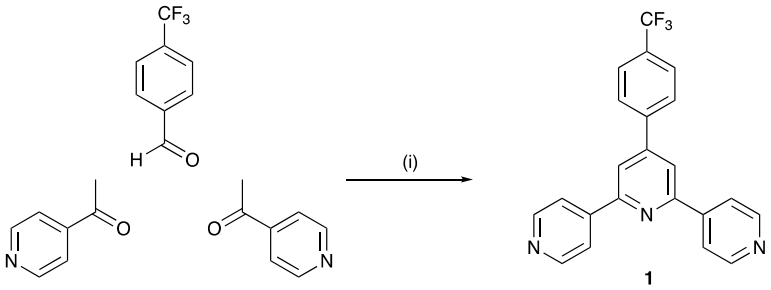

Scheme 4. Synthetic route to ligand **1**. Analogous routes were used for the preparations of **2**, **3**, and **4**. Conditions: (i) KOH, EtOH; NH_3 (aqueous), room temperature, overnight (ca. 21 h).

Compounds **1** and **2** were significantly less soluble in common organic solvents than **3** and **4**, and DMSO-d_6 was used for recording NMR spectra. While **3** and **4** dissolved easily in DMSO-d_6 under ambient conditions, complete dissolution of **1** and **2** was achieved only with heating. Precipitation of **1** in the NMR tube resulted in broadened signals in the ^{1}H NMR spectrum. The ^{1}H and ^{31}C{^{1}H} NMR spectra of compounds **1**–**4** were assigned using 2D-methods, and were consistent with the structures shown in Scheme 3. A singlet at around δ –61 ppm (see Sections 3.2–3.5) was observed in the ^{19}F{^{1}H} NMR spectrum of each compound, consistent with one CF_3 environment. The ^{1}H NMR spectra are compared in Figure S10, while Figure S11 displays the ^{31}C{^{1}H} NMR spectra. While compound **1** is C_2 symmetric on the NMR timescale, the symmetry is lowered on moving the CF_3 substituent from the 4- to 3-position of the 4′-phenyl ring (Figure S10, **1** to **2**). A comparison of the spectra of **1** and **3**, and of **2** and **4** in Figure S10 shows the effects of going from the 4,2′:6′,4″- to 3,2′:6′,3″-tpy domain while retaining the CF_3 group in a common position. Similar effects are seen by comparing the ^{31}C{^{1}H} NMR spectra in Figure S11. The characteristic quartets for C^a (see Scheme 3) with J_{CF} = 272 Hz, and for C^{C3} or C^{C4} (J_{CF} = 31 Hz) are highlighted in Figure S11.

*2.2. Single Crystal Structures of **1** and **2***

Single crystals of **1** were grown by diffusion of Et_2O into a $CHCl_3$ solution of the compound, and X-ray quality crystals of **2** grew as a hot DMSO solution of **2** was allowed to cool to room temperature. Compounds **1** and **2** crystallize in the monoclinic space group $P2_1/c$, and triclinic space group P–1, respectively. The molecular structures of **1**

and one of the two crystallographically independent molecules of **2** are shown in Figure 1a,b, respectively. The conformations of the 4,2′:6′,4″-tpy units differ slightly. In **1**, the angles between the planes of the rings containing N1/N2 and N2/N3 are 31.1 and 2.8°, respectively. In the two independent molecules of **2**, the corresponding angles are 23.2 and 2.4°, and 26.5 and 21.7°. In **1** and molecule 1 of compound **2**, the angle between the planes of the phenyl ring and the central pyridine ring are 33.4 and 35.7°, respectively. These are typical of a 4′-substituted arene ring and minimize unfavorable H...H repulsions. In contrast, the phenyl and central pyridine rings are almost coplanar in the second molecule of **2** (angle between the ring planes = 5.7°). This is associated with face-to-face π-stacking between the independent molecules of **2** which extends across the whole molecular framework shown in Figure 2a. The centroid...centroid separations for pairs of rings containing N3/C33, N2/N5, N1/N4 and N6/C9 are 3.70, 3.67, 3.76, and 3.78 Å, and the corresponding angles between the planes of the stacked rings are 4.9, 3.3, 0.8, and 6.1°. Stacking of molecules continues to assemble columns along the crystallographic *a*-axis (Figure S12). The head-to-tail arrangement of the molecules (Figure 2a) facilitates C–H...F hydrogen bond formation between adjacent molecules which are augmented by C–H...N hydrogen bonds leading to an extended array (Figure 2b). Contact parameters are given in the caption to Figure 2b. Packing of molecules of **1** is also dominated by face-to-face π-stacking, which may contribute to the low solubilities of the compounds. As in **2**, the stacking interaction in **1** extends across the whole molecule, and extended columnar assemblies are formed (Figure 2c). The centroid...centroid distances between pairs of stacked rings containing N3/N3^{i}, N2/N2^{i}, N1/C10^{i} and C10/N1^{i} (symmetry code i = x, $^{3}/_{2}$–y, $-^{1}/_{2}$+z) are 4.0, 4.2, 3.8, 3.7 Å, and the corresponding angles between the ring planes are 5.1, 0.6, 3.1, and 3.1°. Thus, despite the change in the position of the CF_3 substituent on going from **1** to **2**, the structural motifs and packing interactions bear a striking resemblance to one another. These observations complement a recent study by Yi et al. which highlights the scarcity of investigations of π-stacking interactions between trifluoromethylated aromatics [43].

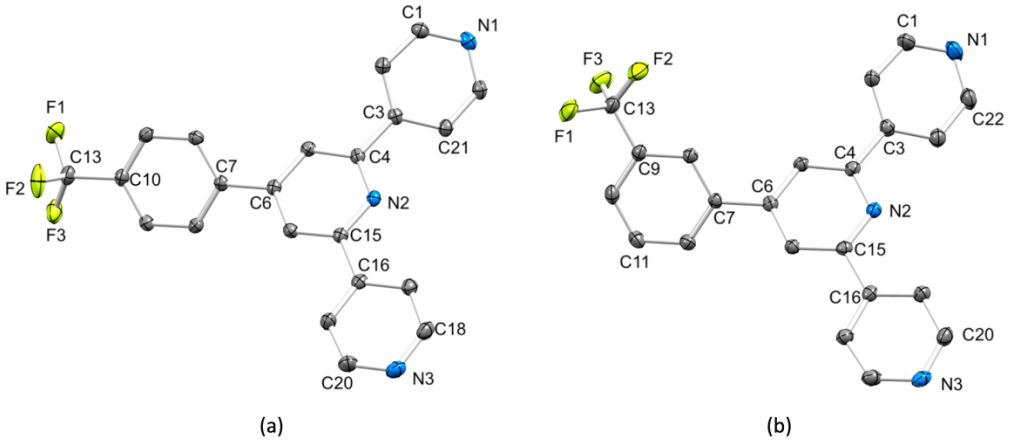

Figure 1. The molecular structures of (**a**) **1** and (**b**) one of the two crystallographically independent molecules of **2**; the structure of the second molecule of **2** is similar to that shown. H atoms are omitted for clarity, and ellipsoids are drawn at 40% probability level. Selected bond lengths for **1**: F1–C13 = 1.3292(16), F2–C13 = 1.3357(16), F3–C13 = 1.3372(16), C10–C13 = 1.4958(17), C6–C7 = 1.4859(16), C4–C3 = 1.4889(16), C15–C16 = 1.4930(17) Å. Selected bond lengths for **2** molecule 1: F1–C13 = 1.339(3), F2–C13 = 1.330(4), F3–C13 = 1.345(4), C9–C13 = 1.496(4), C7–C6 = 1.483(4), C3–C4 = 1.489(4), C15–C16 = 1.494(4) Å; the bond lengths in **2** molecule 2 are similar.

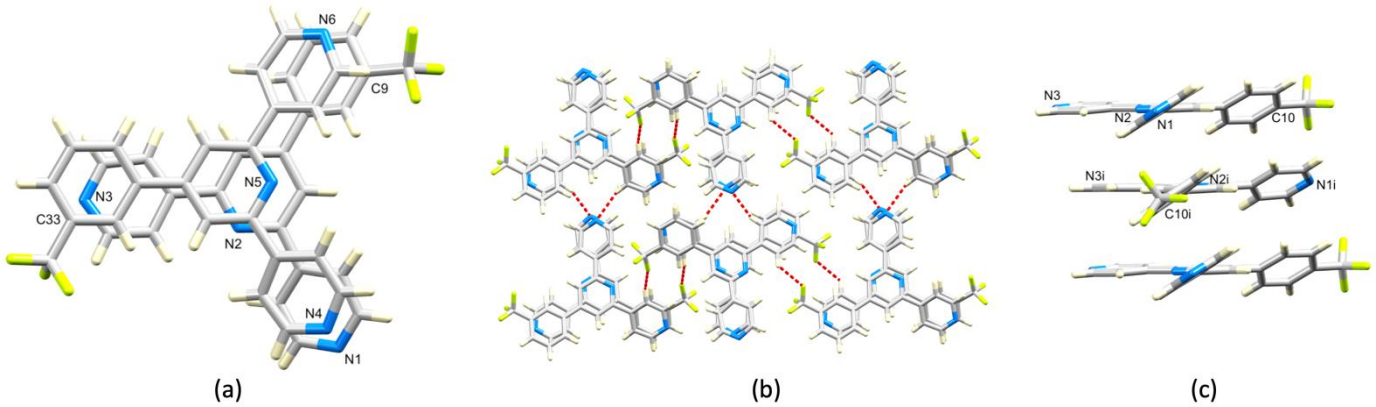

Figure 2. (**a**) Face-to-face π-stacking between the two independent molecules of **2**. (**b**) The π-stacked pairs of molecules of **2** are interconnected by C–H...F and C–H...N interactions: N1...H17^{i}–C17^{i} = 2.59 Å; C19–H19...F4^{ii} = 2.65 Å; F2...H39^{iii}–C39^{iii} = 2.62 Å; N4...H41^{iv}–C41^{iv} = 2.71 Å (symmetry codes i = *x*, 1+*y*, *z*; ii = 1–*x*, 1–*y*, –*z*; iii = 1–*x*, 1–*y*, 1–*z*; iv = *x*, 1+*y*, *z*). (**c**) Face-to-face π-stacking between molecules of **1** leads to columnar assemblies.

2.3. Single-Crystal Structures of the Coordination Polymers $[Cu_2(hfacac)_4(\mathbf{1})_2]_n \cdot 2nC_6H_4Cl_2$, $[Cu(hfacac)_2(\mathbf{2})]_n \cdot 2nC_6H_5Me$, $[Cu_2(hfacac)_4(\mathbf{3})_2]_n \cdot nC_6H_4Cl_2$, $[Cu_2(hfacac)_4(\mathbf{3})_2]_n \cdot nC_6H_5Cl$ and $[Cu(hfacac)_2(\mathbf{4})]_n \cdot nC_6H_5Cl$

Single crystals were grown under ambient conditions by layering a solution of $[Cu(hfacac)_2]\cdot H_2O$ in either toluene, chlorobenzene or 1,2-dichlorobenzene over a chloroform solution of **1**, **2**, **3** or **4**. For each terpyridine ligand, X-ray quality crystals were obtained only for one or two of the solvent combinations, and structural analysis of $[Cu_2(hfacac)_4(\mathbf{1})_2]_n \cdot 2nC_6H_4Cl_2$, $[Cu(hfacac)_2(\mathbf{2})]_n \cdot 2nC_6H_5Me$, $[Cu_2(hfacac)_4(\mathbf{3})_2]_n \cdot nC_6H_4Cl_2$, $[Cu_2(hfacac)_4(\mathbf{3})_2]_n \cdot nC_6H_5Cl$ and $[Cu(hfacac)_2(\mathbf{4})]_n \cdot nC_6H_5Cl$ revealed the assembly of a 1D-coordination polymer in each case. $[Cu_2(hfacac)_4(\mathbf{3})_2]_n \cdot nC_6H_4Cl_2$, $[Cu_2(hfacac)_4(\mathbf{3})_2]_n \cdot nC_6H_5Cl$ both crystallize in the triclinic space group *P*–1 with similar cell dimensions (a = 11.9939(3), b = 12.1658(3), c = 12.9674(3) Å, α = 102.257(2), β = 103.145(2), γ = 91.214(2)° for $[Cu_2(hfacac)_4(\mathbf{3})_2]_n \cdot nC_6H_4Cl_2$, and a = 11.9906(3), b = 11.9911(3), c = 13.0617(3) Å, α = 103.144(2), β = 102.547(2), γ = 91.491(2)° for $[Cu_2(hfacac)_4(\mathbf{3})_2]_n \cdot nC_6H_5Cl$). Since the polymers are essentially isostructural, we discuss only the structure of $[Cu_2(hfacac)_4(\mathbf{3})_2]_n \cdot nC_6H_4Cl_2$.

Figures S13–S16 show the molecular structures of the asymmetric units in $[Cu_2(hfacac)_4(\mathbf{1})_2]_n \cdot 2nC_6H_4Cl_2$, $[Cu(hfacac)_2(\mathbf{2})]_n \cdot 2nC_6H_5Me$, $[Cu_2(hfacac)_4(\mathbf{3})_2]_n \cdot nC_6H_4Cl_2$, and $[Cu(hfacac)_2(\mathbf{4})]_n \cdot nC_6H_5Cl$ with symmetry generated atoms. In all four compounds, each copper(II) center is octahedrally sited with a *trans*-arrangement of pyridine donors. Each of the ligands **1**, **2**, **3**, and **4** coordinates through the outer pyridine rings and links two Cu(II) centers. The bond lengths and angles in the compounds are unexceptional and selected values are given in Table 1. Table 2 presents the angles between the planes of adjacent aromatic rings in each of the coordinated ligands **1**–**4**. The most striking difference is in the angle between the central pyridine ring (with N2) and phenyl ring for the polymer containing **4**. For the compounds containing **1**, **2** and **3**, the twist angles (28.5–34.9°) are typical for minimizing steric interactions between the H atoms on adjacent rings. The near coplanarity of the rings in $[Cu(hfacac)_2(\mathbf{4})]_n \cdot nC_6H_5Cl$ appears to be associated with a combination of effects which are connected to the conformation of the 3,2′:6′,3″-tpy unit (see later). The four structures are discussed below in a comparative way with a focus on the effects of changing the substitution position of the CF_3 group while retaining the same terpyridine isomer, and the effects of going from the 4,2′:6′,4″-tpy to 3,2′:6′,3″-tpy metal-binding domain.

Table 1. Space groups and selected bond lengths and angles in the copper(II) coordination polymers.

Compound	Space Group	Cu–N/Å	Cu–O/Å	N–Cu–O/°
$[Cu_2(hfacac)_4(\mathbf{1})_2]_n \cdot 2nC_6H_4Cl_2$	*Pbca*	2.014(2), 2.016(2)	1.967(2), 1.982(2), 2.298(2), 2.302(2)	91.38(9), 89.24(9), 91.35(9), 88.05(9), 88.83(9), 88.02(9), 91.74(9), 91.37(9)
$[Cu(hfacac)_2(\mathbf{2})]_n \cdot 2nC_6H_5Me$	*Cc*	2.002(6), 2.012(6)	2.046(6), 2.197(6), 2.031(6), 2.234(6)	90.6(2), 90.0(2), 89.5(2), 89.1(2), 90.1(2), 90.6(2), 89.8(2), 90.3(2)
$[Cu_2(hfacac)_4(\mathbf{3})_2]_n \cdot nC_6H_4Cl_2$	*P*–1	2.064(3), 2.023(4)	1.955(3), 2.339(3), 1.990(3), 2.275(3)	88.70(12), 91.30(12), 98.90(12), 81.10(12), 92.38(13), 87.62(13), 88.12(13), 91.88(13)
$[Cu(hfacac)_2(\mathbf{4})]_n \cdot nC_6H_5Cl$	*Pnma*	2.051(3)	1.971(2), 2.291(3)	91.19(10), 88.81(10), 95.60(10), 84.40(10)

Table 2. Angles between the planes of pairs of connected rings in coordinated ligands **1**–**4**.

Compound	Angle between Planes of Adjacent Pyridine Rings/°	Angle between Ring with N2 and Phenyl Ring/°
$[Cu_2(hfacac)_4(\mathbf{1})_2]_n \cdot 2nC_6H_4Cl_2$	12.9, 23.6	28.5
$[Cu(hfacac)_2(\mathbf{2})]_n \cdot 2nC_6H_5Me$	7.8, 26.7	34.9
$[Cu_2(hfacac)_4(\mathbf{3})_2]_n \cdot nC_6H_4Cl_2$	15.7, 21.7	30.0
$[Cu(hfacac)_2(\mathbf{4})]_n \cdot nC_6H_5Cl$	16.6, 16.6	0.9

Ligand **1** presents a V-shaped building block and, combined with the *trans*-arrangement of the pyridine donors in the Cu(II) coordination sphere, this leads to a zigzag 1D-polymer chain in $[Cu_2(hfacac)_4(\mathbf{1})_2]_n \cdot 2nC_6H_4Cl_2$ (Figure 3a). The chains associate through short C–F...F–C interactions (Figure 3b) with F...F distances of 2.92, 2.97, 2.76 and 2.93 Å, which are less than or similar to the sum of the van der Waals radii (2.92–2.94 Å) [44,45]. These contacts involve the ordered CF_3 groups containing C13, C27 and C32 (Figure S13). Although distinct from halogen bonds [46], weak F...F contacts are recognized as contributing towards crystal packing interactions [43,47,48]. At first glance, the packing shown in Figure 3b appears to be reminiscent of the characteristic nesting of zigzag chains in $[Cu_2(\mu\text{-}OAc)_4(4'\text{-}X\text{-}4,2':6',4''\text{-}tpy)]_n$ to form 2D-sheets [11,13,14]. However, the chains in $[Cu_2(hfacac)_4(\mathbf{1})_2]_n \cdot 2nC_6H_4Cl_2$ are offset (highlighted in red in Figure 3c) and a second set of chains slices obliquely through the first as shown in Figure 3c. Interestingly, π-stacking interactions between ligands **1** do not contribute to the packing interactions, although the 1,2-dichlorobenzene solvate molecule does form face-to-face π-stacking contacts with the central pyridine ring of **1** (centroid ... centroid = 3.78 Å, angle between the ring planes = 3.0°).

A zigzag polymer is also present in $[Cu(hfacac)_2(\mathbf{2})]_n \cdot 2nC_6H_5Me$ (Figure 4a, and as in $[Cu_2(hfacac)_4(\mathbf{1})_2]_n \cdot 2nC_6H_4Cl_2$, the dominant packing interactions in $[Cu(hfacac)_2(\mathbf{2})]_n \cdot 2n$ C_6H_5Me are weak C–F...F–C contacts. Four of the five crystallographically independent CF_3 groups are involved in such interactions, and these CF_3 units are ordered. The C–F...F–C network in $[Cu(hfacac)_2(\mathbf{2})]_n \cdot 2nC_6H_5Me$ is more complex than in the polymer containing ligand **1**, with each F atom of the CF_3 group in **2** forming a C–F...F–C contact with an {$Cu(hfacac)_2$} unit in a different polymer chain (Figure 4b,c). The F...F distances for these interactions are 2.94, 2.92 and 2.82 Å. The 1D-polymers are arranged parallel to one another (Figure 4c, and Figure S17 in the Supporting Material). As in $[Cu_2(hfacac)_4(\mathbf{1})_2]_n \cdot 2nC_6H_4Cl_2$, there are no π-stacking interactions between arene rings in adjacent chains in $[Cu(hfacac)_2(\mathbf{2})]_n \cdot 2nC_6H_5Me$. It is tempting to suggest that this is due to the steric hindrance of the {$Cu(hfacac)_2$} domains. We note that there are also no π-stacking

interactions between 4,2′:6′,4″-tpy domains in the 1D-polymers $[Cu(hfacac)_2(L_2)]_n \cdot CHCl_3$ and $[Cu(hfacac)_2(L_4)]_n$ (see Scheme 2 for L_2 and L_4) [36], although Moreno and coworkers did observe π-stacking of 4,2′:6′,4″-tpy units in the molecular complex $[Cu_3(ttfacac)_6(L_1)_2]$ (L_1, see Scheme 2) [37]. Another similarity between $[Cu_2(hfacac)_4(\mathbf{1})_2]_n \cdot 2nC_6H_4Cl_2$ and $[Cu(hfacac)_2(\mathbf{2})]_n \cdot 2nC_6H_5Me$ is the role of the solvent molecules. In the latter, one toluene molecule engages in a face-of-face π-stacking interaction with one pyridine ring of **2** (centroid … centroid = 3.71 Å, angle between the ring planes = 2.7°). Additionally, the same pyridine ring (with N1) exhibits a CH... π contact with the second toluene molecule (C–H...centroid = 2.95 Å, angle C–H...centroid = 149.3°).

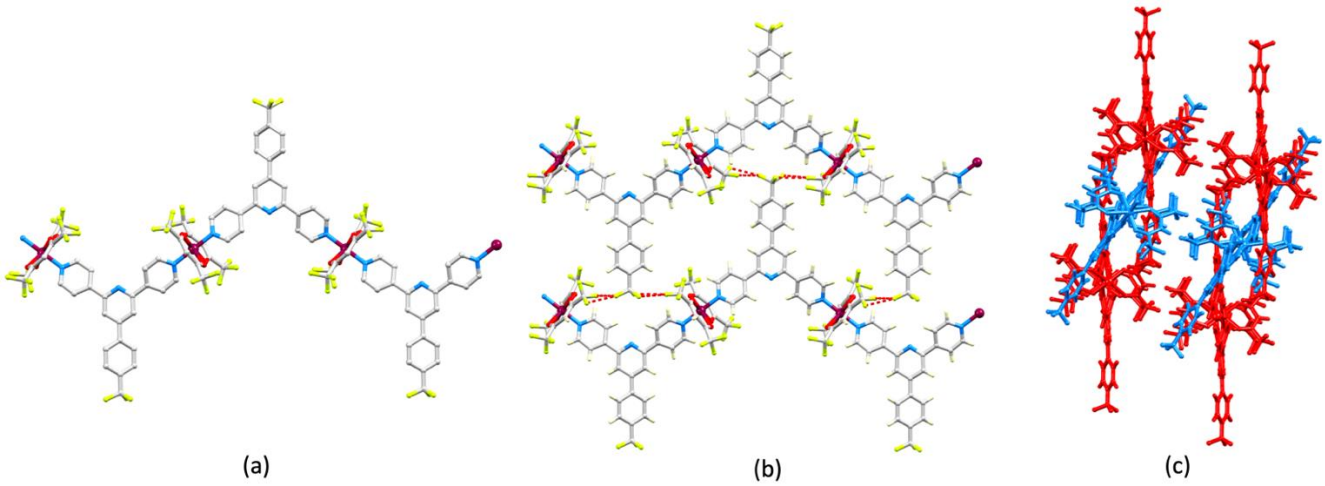

Figure 3. The structure of $[Cu_2(hfacac)_4(\mathbf{1})_2]_n \cdot 2nC_6H_4Cl_2$. (**a**) Part of one 1D-polymer with H atoms omitted. (**b**) Chains associate through short C–F...F–C contacts (hashed red lines). (**c**) The chains shown in (**b**) are offset (two pairs are shown in red) and a second set of chains (in blue) slices obliquely through the first.

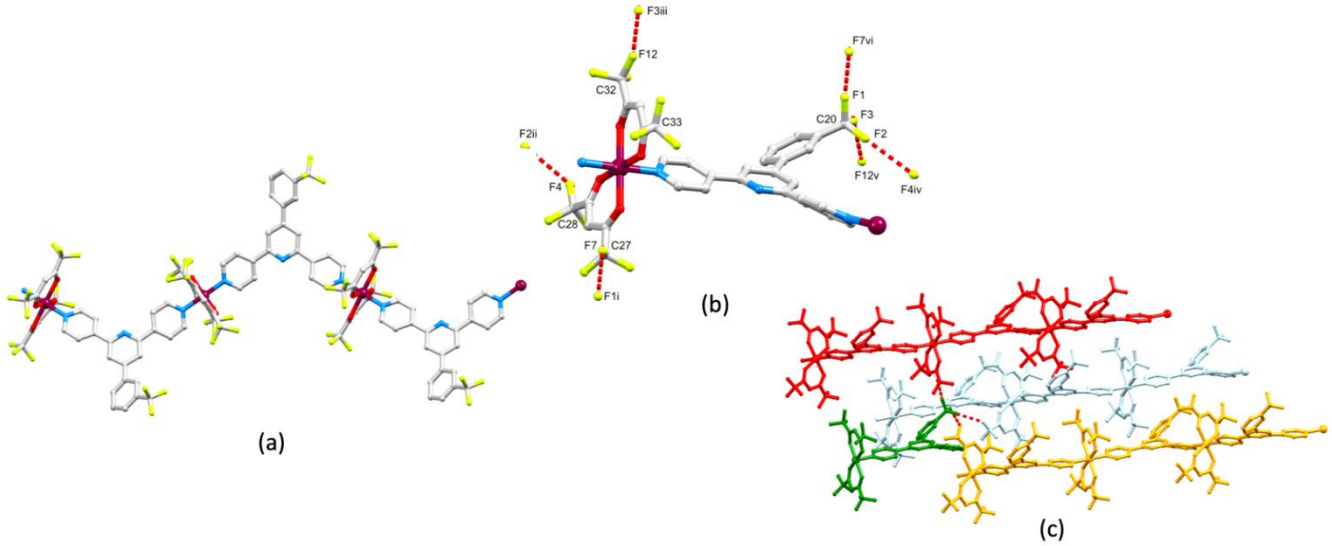

Figure 4. The structure of $[Cu(hfacac)_2(\mathbf{2})]_n \cdot 2nC_6H_5Me$. (**a**) Part of one 1D-polymer with H atoms omitted. (**b**) Four of the five CF_3 groups are involved in C–F...F–C interactions and this leads to (**c**) the CF_3 group in **2** being linked to three different polymer chains; the asymmetric unit is shown in green. Symmetry codes: i = $^3/_2+x$, $^1/_2+y$, z; ii = $^3/_2+x$, $-^3/_2-y$, $^1/_2+z$; iii = $^1/_2+x$, $-^3/_2-y$, $^1/_2+z$; iv = $-^3/_2+x$, $-^3/_2-y$, $-^1/_2+z$; v = $-^1/_2+x$, $-^3/_2-y$, $-^1/_2+z$; vi = $-^3/_2+x$, $-^1/_2+y$, z.

Having investigated the effects of moving the substitution position of the CF_3 group while retaining a 4,2′:6′,4″-tpy metal-binding unit on going from **1** to **2**, we turned our attention to ligands **3** and **4** with 3,2′:6′,3″-tpy domains. $[Cu_2(hfacac)_4(\mathbf{3})_2]_n \cdot nC_6H_4Cl_2$

crystallizes in the triclinic space group *P*–1 with one independent ligand **3** and two half-{Cu(hfacac)$_2$} units, with each of Cu1 and Cu2 lying on an inversion center. Figure 5a displays part of the 1D-polymer chain present in the structure, and shows the octahedral Cu(II) coordination geometry. The 3,2′:6′,3″-tpy unit adopts conformation **C** in Scheme 1, and the alternating arrangement of these units along the chain is dictated by symmetry. As we have previously discussed [15], for a *trans*-arrangement of pyridine donors at a metal center, ligand conformation **C** can, in principle, lead to assembly algorithms **I**, **II** or **III** (Scheme 5) of which two are represented in [Cu$_2$(hfacac)$_4$(**3**)$_2$]$_n$·*n*C$_6$H$_4$Cl$_2$ (Figure 5a).

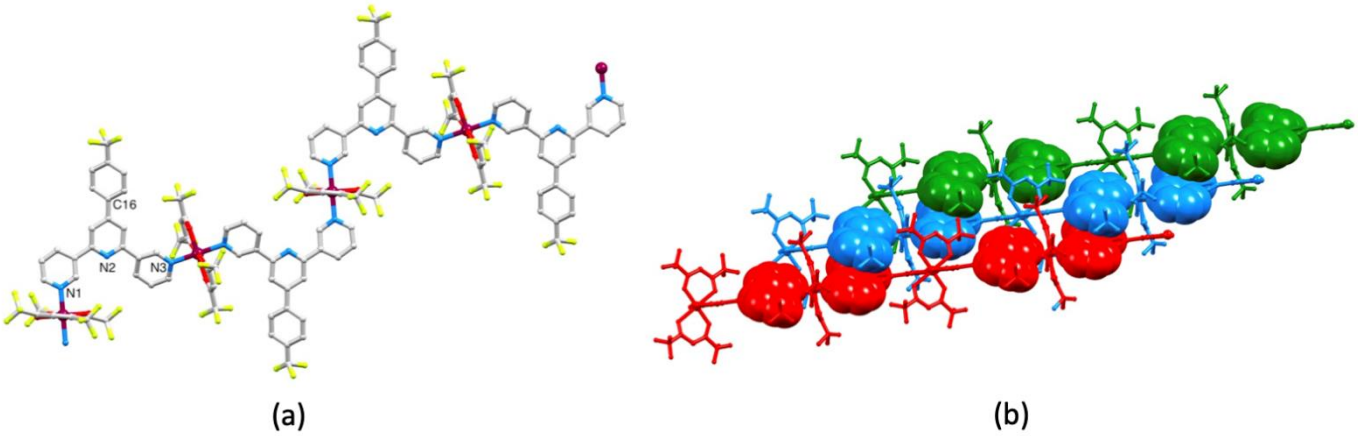

Figure 5. The structure of [Cu$_2$(hfacac)$_4$(**3**)$_2$]$_n$·*n*C$_6$H$_4$Cl$_2$. (**a**) Part of the 1D-coordination polymer showing that the 3,2′:6′,3″-tpy unit exhibits conformation **C** (see Scheme 1) and the two crystallographically different Cu centers (compare with Scheme 5). (**b**) Stacking interactions between adjacent 1D-polymers.

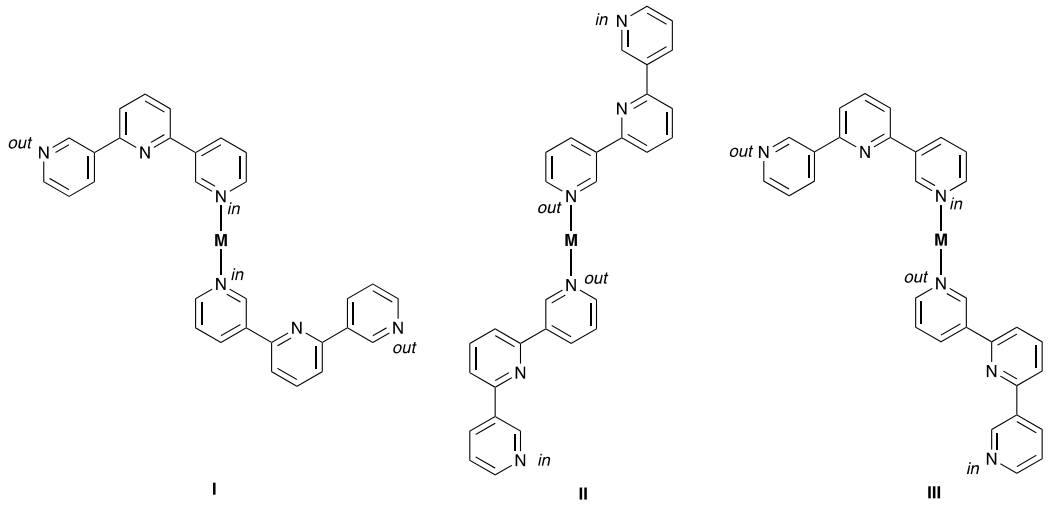

Scheme 5. With 3,2′:6′,3″-tpy in conformation **C** (Scheme 1), three coordination patterns are possible for a *trans*-arrangement of ligands at a metal center. We have previously [15] used the labels in and out to describe the orientation of the lone pair of each coordinating N atom with respect to the central pyridine ring.

Compared to the assemblies with ligands **1** and **2**, a major difference in the packing polymer chains in [Cu$_2$(hfacac)$_4$(**3**)$_2$]$_n$·*n*C$_6$H$_4$Cl$_2$ (and also in the polymer with **4**, see below) is the role of face-to-face π-stacking interactions. The change in the relative positions of the {Cu(hfacac)$_2$} units caused by a change in the positions of the *N*-donors on going from **1** and **2** to **3**, may alleviate steric congestion, allowing a closer approach of the arene units. Figure 5b depicts the centrosymmetric pairing of 3,2′:6′,3″-tpy units in adjacent chains with the pyridine ring containing N1 engaging in a π-π stack with the phenyl ring with atom C16

(symmetry code = 2–*x*, 1–*y*, 1–*z*). The centroid...centroid distance is 3.82 Å, and the angle between the ring planes is 18.7°. As Figure 5b shows, the stacking interactions interconnect 1D-polymers through the lattice. Additional π-stacking interactions are provided by the 1,2-$C_6H_4Cl_2$ molecule which resides over the pyridine rings containing N2 and N3. This mirrors the role of the aromatic solvent in the assemblies with ligands **1** and **2**. These interactions are supplemented by extensive C–F...F–C and C–F...H–C contacts (Figure S18 in the Supplementary Materials). The C–F...F–C distances are 2.85 and 2.87 Å, which are within the sum of the van der Waals radii (2.92–2.94 Å) [44,45]. The shortest H...F contacts lie in the range 2.50–2.57 Å, which compare with 2.67 Å using Bondi's van der Waals radii [44] or 2.57 Å using radii recommended by Rowland and Taylor [45]. Longer H...F contacts (>2.64 Å) have not been included in Figure S18. We note that disordering of some CF_3 groups (see Figure S15) precludes a detailed discussion of interactions involving these units.

[Cu(hfacac)$_2$(**4**)]$_n$·*n*C_6H_5Cl crystallizes in the orthorhombic space group *Pmna* and the asymmetric unit contains half of a molecule of **4**, the second half being generated by a mirror plane. Consequently, the CF_3 group in **4** is disordered over two sites (see Section 3.11) and in the figures and discussion below, only one of these sites is considered. Figure 6a shows part of the 1D-polymer chain. The 3,2′:6′,3″-tpy adopts conformation **A** in Scheme 1 and, as noted earlier, the near coplanarity of the rings containing N2 and C6 (Figure S16 and Table 2) is striking. This can be traced back to the accommodation of the 3-$CF_3C_6H_4$ ring within a pocket between two {Cu(hfacac)$_2$} units which follows from the conformation of the 3,2′:6′,3″-tpy. This leads to the presence of short intramolecular C–H...F–C interactions between the *ortho*-H atoms of the phenyl ring and CF_3 groups (which are ordered) of the two {Cu(hfacac)$_2$} units (Figure 6b). The H4...F6 and H7...F6 distances are 2.68 and 2.45 Å, respectively, with C–H...F angles of 154.1 and 152.3°, respectively. The shorter contact is well within the lower (see above) estimate of the sum of the van der Waals radii (2.57 Å [45]) and is towards the shorter end of the range of contacts seen in a survey of the CSD reported in 2005 [48]. The 1D-polymers associate through face-to-face π-stacking of phenyl and central-pyridine rings (angle between ring planes = 0.9°, cenroid...centroid = 3.72 Å) as depicted in Figure 6c, and the interactions extend infinitely through the lattice (Figure S19). The arrangement of neighboring stacks allows association through C–H...π contacts (Figure 6d) with the C–H_{phenyl}...$centroid_{phenyl}$ distance being 3.15 Å. The role of the chlorobenzene solvent could not be assessed because of disordering (see Section 3.11).

2.4. PXRD Analysis

After single crystals had been selected for single-crystal X-ray structure determination, the remaining crystals in each crystallization tube were collected and were washed with $CHCl_3$ and the aromatic solvent used in the crystallization experiment (toluene, chlorobenzene or 1,2-dichlorobenzene). The bulk samples were analyzed by IR spectroscopy and PXRD. The IR spectra are shown in Figures S20–S23 in the Supporting Materials. When compared to the IR spectra of ligands **1**–**4**, a strong absorption is observed in the spectra of the coordination polymers containing **1**, **2**, **3**, and **4**, respectively, at 1653, 1650, 1650 and 1646 cm^{-1} which is absent in the spectra of the ligands. This is assigned to one of the C=O stretching modes which appear at 1644 and 1614 cm^{-1} in [Cu(hfacac)$_2$] [49].

Confirmation that the single crystals selected were representative of the bulk crystalline materials came from a comparison of the experimental PXRD patterns (shown in red in Figure 7a–d) with the patterns predicted from the single crystal structures (black traces in Figure 7). For each coordination polymer, all peaks in the predicted pattern had a matching partner in the experimental PXRD pattern, and no additional peaks were observed. The differences in intensities (blue traces in Figure 7) can be justified in terms of differences in the preferred orientations of the crystallites in the bulk powder samples.

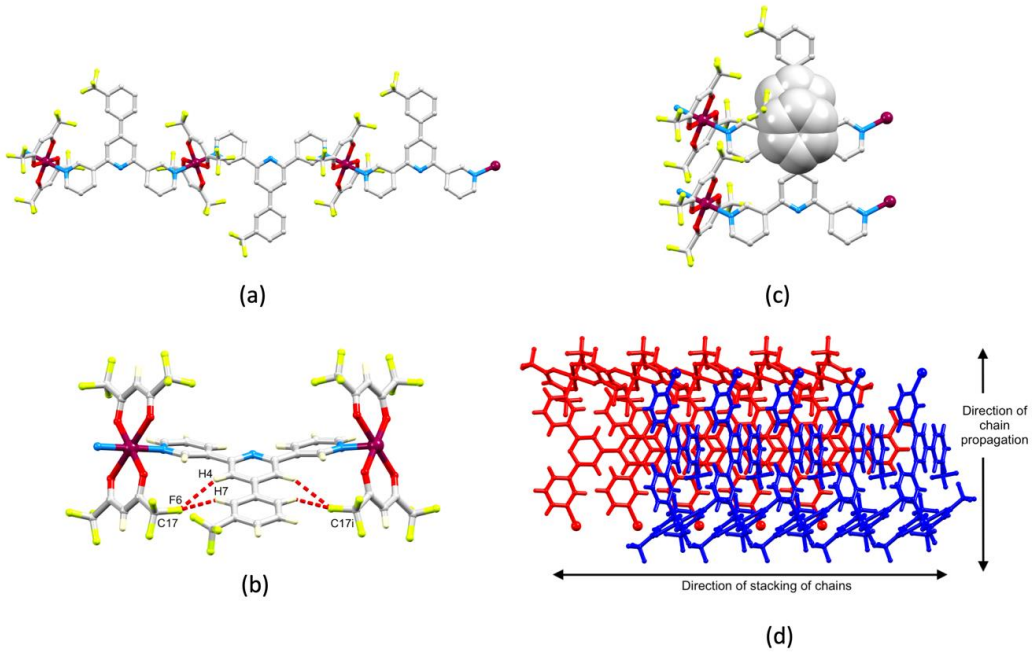

Figure 6. The structure of [Cu(hfacac)$_2$(**4**)]$_n$·*n*C$_6$H$_5$Cl. (**a**) Part of the 1D-polymer. The CF$_3$ group in **4** is disordered over two sites related by a mirror plane and only one position is shown. (**b**) Intramolecular C–H...F–C contacts; symmetry code i = *x*, $^3/_2$–*y*, *z*. (**c**) π-Stacking between the phenyl ring and the pyridine ring containing N2^{ii} (symmetry code ii = 1+*x*, *y*, *z*). (**d**) The arrangement of adjacent stacks of polymer chains.

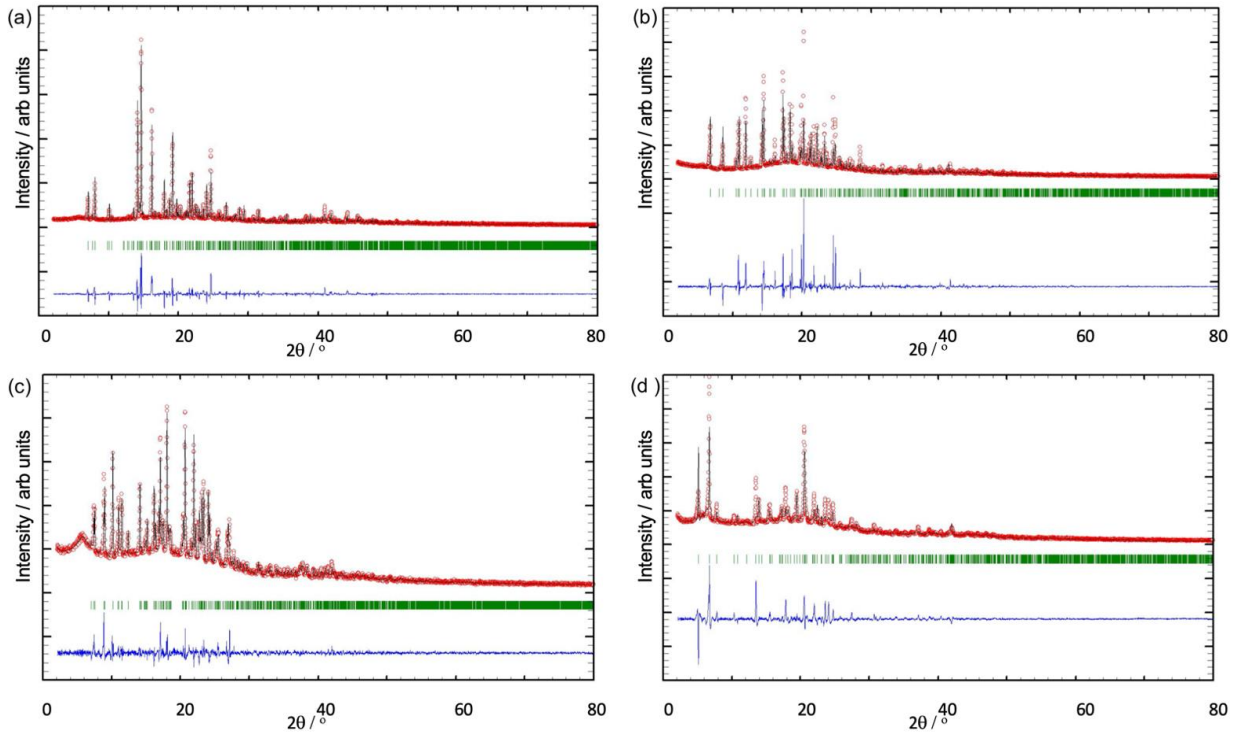

Figure 7. X-Ray diffraction (CuKα1 radiation) patterns (red circles) of the bulk crystalline materials of (**a**) [Cu2(hfacac)4(**1**)2]*n*·2*n*C6H4Cl$_2$, (**b**) [Cu(hfacac)$_2$(**2**)]$_n$·2*n*C$_6$H$_5$Me, (**c**) [Cu$_2$(hfacac)$_4$(**3**)$_2$]$_n$·nC$_6$H$_4$Cl$_2$, and (**d**) [Cu$_2$(hfacac)$_4$(**4**)]$_n$·*n*C$_6$H$_5$Cl, fitting to the predicted patterns from the single-crystal structures. The black lines are the best fits from the Rietveld refinements, and green lines display the Bragg peak positions. Each blue plot gives the difference between calculated and experimental points (see text).

2.5. Preparative Scale Reactions

To complete the investigation, we performed preparative scale syntheses of the copper(II) complexes using a 1:1 ratio of $[Cu(hfacac)_2]\cdot H_2O$ to ligand **1**, **2**, **3** and **4**. A solution of $[Cu(hfacac)_2]\cdot H_2O$ in toluene, chlorobenzene or 1,2-dichlorobenzene was added to a chloroform solution of each ligand and the green precipitates that formed were isolated and dried under vacuum. Satisfactory elemental analyses were obtained for $[Cu_2(hfacac)_4(\mathbf{1})_2]_n\cdot n C_6H_4Cl_2$, $[Cu(hfacac)_2(\mathbf{2})]_n$, $[Cu(hfac)_2(\mathbf{3})]_n$, and $[Cu(hfacac)_2(\mathbf{4})]_n$. A PXRD pattern was measured for each compound, and comparisons of these experimental data with the patterns from the bulk crystalline materials from single-crystal growth are displayed in Figure 8 and Figures S24–S26. Good matches are seen for all compounds, providing support that the same coordination polymers are produced on a preparative scale as in single-crystal growth under conditions of layering.

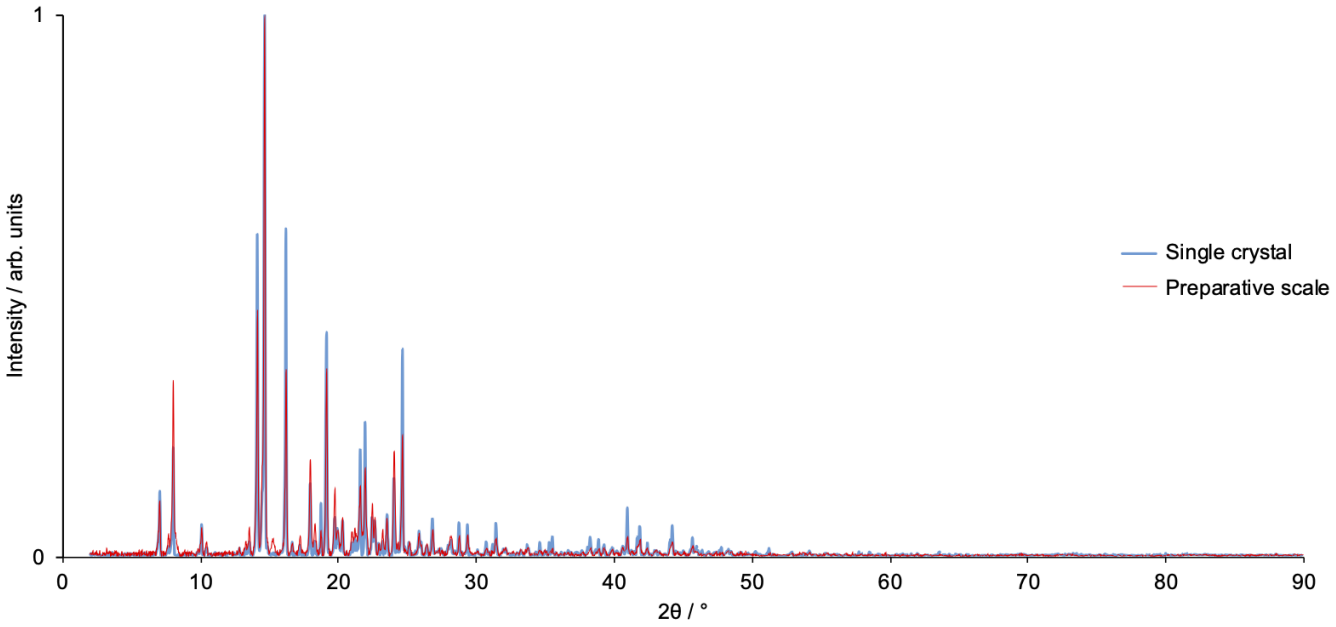

Figure 8. A comparison of the PXRD pattern of $[Cu_2(hfacac)_4(\mathbf{1})_2]_n\cdot n C_6H_4Cl_2$ prepared on a preparative scale, and that of the bulk single crystals of $[Cu_2(hfacac)_4(\mathbf{1})_2]_n\cdot 2n C_6H_4Cl_2$. The difference in solvent arises from drying the synthesized material.

3. Materials and Methods

3.1. General

3-Acetylpyridine and 4-trifluoromethylbenzaldehyde were purchased from Acros Organics (Fisher Scientific AG, 4153 Reinach, Switzerland). 4-Acetylpyridine was bought from Sigma Aldrich (Riedstr. 2, 89555 Steinheim, Germany), 4-trifluoromethylbenzaldehyde from Fluorochem Ltd. (Glossop, UK) and $Cu(hfacac)_2$ monohydrate was bought from abcr GmbH (Im Schlehert 10, 76187 Karlsruhe, Germany). All chemicals were used as received. Analytical thin-layer chromatography was conducted with pre-coated silica gel 60 F_{254} aluminium sheets (Merck KGaA, 64293 Darmstadt, Germany) and visualized using ultraviolet (UV) light (254 nm). Flash column chromatography was performed on a Biotage Selekt system (Biotage, 75103 Uppsala, Sweden) with self-packed silica gel columns (SiliaFlash® P60, 40–63 µm, 230-400 mesh from SiliCycle Inc., Québec, QC, Canada) using ethyl acetate in cyclohexane (gradient) as eluent and monitoring and collecting at 254 nm.

^1H and $^{13}C\{^1H\}$ NMR spectra were recorded on a Bruker Avance III-500 spectrometer (Bruker BioSpin AG, 8117 Fällanden, Switzerland) at 298 K. The ^1H and ^{13}C NMR chemical shifts were referenced with respect to the residual solvent peak (δ 2.50 and δ 39.52 respectively for DMSO-d6). $^{19}F\{^1H\}$ NMR spectra were recorded at 298 K on a Bruker Avance III-600 spectrometer (Bruker BioSpin AG, 8117 Fällanden, Switzerland). MALDI-

TOF mass spectra were recorded on a Shimadzu MALDI 8020 (Shimadzu Schweiz GmbH, 4153 Reinach, Switzerland) using α-cyano-4-hydroxycinnamic acid as matrix. PerkinElmer UATR Two (Perkin Elmer, 8603 Schwerzenbach, Switzerland) and Cary-5000 (Agilent Technologies Inc., Santa Clara, CA 95051, US) instruments were used to record FT-infrared (IR) and UV-VIS absorption spectra, respectively. Melting temperatures were determined using a Stuart melting point SMP 30 device (Cole-Parmer, Stone, UK).

*3.2. 4′-(4-(Trifluoromethyl)Phenyl)-4,2′:6′,4″-Terpyridine (**1**)*

4-Trifluoromethylbenzaldehyde (1.74 g, 10.0 mmol, 1.0 eq) was dissolved at room temperature in EtOH (50 mL). 4-Acetylpyridine (2.8 mL, 25.0 mmol, 2.5 eq) and crushed KOH (1.12 g, 20.0 mmol, 2.0 eq) were then added to the colorless solution. Immediate color change upon the addition of KOH from colorless to orange observed. Then slow addition of aqueous NH_3 (32%, 38.5 mL) followed. The reaction mixture was stirred at room temperature overnight (21 h). The precipitate was collected by filtration and washed with H_2O (3 × 10 mL) followed by EtOH (3 × 10 mL). The light red solid was reprecipitated from a MeOH (40 mL)/CH_2Cl_2 (1 mL)/ and chloroform (1 mL) mixture and dried *in vacuo* overnight yielding **1** (1.39 g, 3.68 mmol, 36.8%) as a colorless solid. M.p. 266.7–268.7 °C. ^{1}H NMR (500 MHz, DMSO-d6): δ/ppm 8.79 (m, 4H, H^{A2}), 8.56 (s, 2H, H^{B3}), 8.34 (m, 6H, H^{A3+C2}), 7.96 (d, J = 8.0 Hz, 2H, H^{C3}). ^{13}C{^{1}H} NMR (126 MHz, DMSO-d6): δ/ppm 154.5 (C^{B2}), 150.4 (C^{A2}), 148.8 (C^{B4}), 145.1 (C^{A4}), 141.0 (C^{C1}), 129.8 (q, J_{CF} = 31 Hz, C^{C4}), 128.5 (C^{C2}), 125.9 (q, J_{CF} = 4 Hz, C^{C3}), 124.1 (q, J_{CF} = 272 Hz, C^{a}), 121.2 (C^{A3}), 119.4 (C^{B3}). ^{19}F{^{1}H} NMR (565 MHz, DMSO-d6): δ/ppm −61.1. UV-VIS (MeCN, 2.0 × 10^{-5} mol dm^{-3}) λ/nm 250 (ε/dm^{-3} mol^{-1} cm^{-1} 42,420), 306 (7600). MALDI-TOF-MS *m/z* 378.10 $[M+H]^+$ (calc. 378.12). Found C 69.98, H 3.81, N 11.17; required for $C_{22}H_{14}F_3N_3$ C 70.02, H 3.74, N 11.14. See Figure S5 for the IR spectrum of **1**.

Single crystals of **1** were grown as follows. Ligand **1** (ca. 10 mg) was added to $CHCl_3$ (2 mL) in a small vial to give a clear solution. The open vial was then placed in a larger vial containing Et_2O. Slow diffusion of the non-solvent led to colorless plate-shaped crystals after 7 days.

*3.3. 4′-(3-(Trifluoromethyl)Phenyl)-4,2′:6′,4″-Terpyridine (**2**)*

3-Trifluoromethylbenzaldehyde (1.74 g, 10.0 mmol, 1.0 eq) was dissolved at room temperature in EtOH (50 mL). 4-Acetylpyridine (2.8 mL, 25.0 mmol, 2.5 eq) and crushed KOH (1.12 g, 20.0 mmol, 2.0 eq) were then added to the colorless solution. Immediate color change upon the addition of KOH from colorless to orange was observed. Then slow addition of aqueous NH_3 (32%, 38.5 mL) followed. The reaction mixture was stirred at room temperature overnight (21 h). The formed precipitate was collected by filtration and washed with H_2O (3 x 10 mL) followed by EtOH (3 × 10 mL). The light brown solid was reprecipitated from a MeOH (40 mL)/ CH_2Cl_2 (1 mL) and chloroform (1 mL) mixture and dried in vacuo overnight affording **2** (1.86 g, 4.93 mmol, 49.3%) as a colorless solid. M.p. 237.0–239.4 °C. ^{1}H NMR (500 MHz, DMSO-d6): δ/ppm 8.78 (m, 4H, H^{A2}), 8.57 (s, 2H, H^{B3}), 8.47 (s, 1H, H^{C2}), 8.42 (d, J = 8.4 Hz, 1H, H^{C6}), 8.36 (m, 4H, H^{A3}), 7.91 (d, J = 7.7 Hz, 1H, H^{C4}), 7.83 (t, J = 7.8 Hz, 1H, H^{C5}). ^{13}C{^{1}H} NMR (126 MHz, DMSO-d6): δ/ppm 154.6 (C^{B2}), 150.4 (C^{A2}), 148.8 (C^{B4}), 145.1 (C^{A4}), 138.0 (C^{C1}), 132.6 (C^{C6}), 130.1 (C^{C5}), 130.0 (q, J_{CF} = 31 Hz, C^{C3}), 126.2 (q, J_{CF} = 4 Hz, C^{C4}), 124.3 (q, J_{CF} = 4 Hz, C^{C2}), 124.1 (q, J_{CF} = 272 Hz, C^{a}), 121.2 (C^{A3}), 119.3 (C^{B3}). ^{19}F{^{1}H} NMR (565 MHz, DMSO-d6): δ/ppm −60.7. UV-VIS (MeCN, 2.0 × 10^{-5} mol dm^{-3}) λ/nm 250 (ε/dm^{-3} mol^{-1} cm^{-1} 42,270), 294 (7300). MALDI-TOF-MS *m/z* 378.15 $[M+H]^+$ (calc. 378.12). Found C 70.06, H 3.95, N 11.31; required for $C_{22}H_{14}F_3N_3$ C 70.02, H 3.74, N 11.14. See Figure S6 for the IR spectrum of **2**.

Single crystals of **2** were grown as follows. Compound **2** (ca. 10 mg) was added to DMSO (0.7 mL) in an NMR tube to give a white suspension. The NMR tube was then heated using a heat gun to give a clear solution, and as the solution was allowed to cool to room temperature, colorless plate-shaped crystals grew within an hour.

*3.4. 4′-(4-(Trifluoromethyl)Phenyl)-3,2′:6′,3″-Terpyridine (**3**)*

4-Trifluoromethylbenzaldehyde (1.74 g, 10.0 mmol, 1.0 eq) was dissolved at room temperature in EtOH (50 mL). 3-Acetylpyridine (2.8 mL, 25.0 mmol, 2.5 eq) and crushed KOH (1.12 g, 20.0 mmol, 2.0 eq) were then added to the light yellow solution. Immediate color change upon the addition of KOH from yellow to orange was observed. Then slow addition of aqueous NH_3 (32%, 38.5 mL) followed. The reaction mixture was stirred at room temperature overnight (24 h). The formed precipitate was collected by filtration and washed with H_2O (3 × 10 mL) followed by EtOH (3 × 10 mL). Purification by column chromatography (380 g self-packed silica gel column, Biotage Select, eluent: EtOAc in cyclohexane 20–100%) gave **3** (1.56 g, 4.12 mmol, 41.2%) as a colorless crystalline solid. M.p. 209.4–211.3 °C. ^{1}H NMR (500 MHz, DMSO-d6): δ/ppm 9.53 (dd, J = 2.3, 0.7 Hz, 2H, H^{A2}), 8.73–8.70 (m, 4H, H^{A4+A6}), 8.44 (s, 2H, H^{B3}), 8.33 (d, J = 8.1 Hz, 2H, H^{C2}), 7.94 (d, J = 8.3 Hz, 2H, H^{C3}), 7.59 (m, 2H, H^{A5}). $^{13}C\{^1H\}$ NMR (126 MHz, DMSO-d6): δ/ppm 154.8 (C^{B2}), 150.2 (C^{A6}), 148.4 (C^{B4}), 148.3 (C^{A2}), 141.2 (q, J_{CF} = 1 Hz, C^{C1}), 134.5 (C^{A4}), 133.8 (C^{A3}), 129.7 (q, J_{CF} = 31 Hz, C^{C4}), 128.5 (C^{C2}), 125.8 (q, J_{CF} = 4 Hz, C^{C3}), 124.1 (q, J_{CF} = 272 Hz, C^a), 123.8 (C^{A5}), 117.9 (C^{B3}). $^{19}F\{^1H\}$ NMR (565 MHz, DMSO-d6): δ/ppm −61.0. UV-VIS (MeCN, 2.0 × 10^{-5} mol dm^{-3}) λ/nm 249 (ε/dm^{-3} mol^{-1} cm^{-1} 43,620), 297 (6550). MALDI-TOF-MS *m/z* 378.09 $[M+H]^+$ (*calc.* 378.12). Found C 69.89, H 3.82, N 11.50; required for $C_{22}H_{14}F_3N_3$ C 70.02, H 3.74, N 11.14. See Figure S7 for the IR spectrum of **3**.

*3.5. 4′-(3-(Trifluoromethyl)Phenyl)-3,2′:6′,3″-Terpyridine (**4**)*

3-Trifluoromethylbenzaldehyde (1.74 g, 10.0 mmol, 1.0 eq) was dissolved at room temperature in EtOH (50 mL). 3-Acetylpyridine (2.8 mL, 25.0 mmol, 2.5 eq) and crushed KOH (1.12 g, 20.0 mmol, 2.0 eq) were then added to the light yellow solution. Immediate color change upon the addition of KOH from yellow to orange was observed. Then slow addition of aqueous NH_3 (32%, 38.5 mL) followed. The reaction mixture was stirred at room temperature overnight (24 h). The formed precipitate was collected by filtration and washed with H_2O (3 × 10 mL) and EtOH (3 × 10 mL). The product was recrystallized from MeOH and dried in vacuo to yield **4** (1.18 g, 3.13 mmol, 31.3%) as a colorless solid. M.p. 165.3–167.0 °C. ^{1}H NMR (500 MHz, DMSO-d6): δ/ppm 9.55 (dd, J = 2.3, 0.8 Hz, 2H, H^{A2}), 8.73 (dt, J = 7.9, 2.0 Hz, 2H, H^{A4}), 8.70 (dd, J = 4.8, 1.6 Hz, 2H, H^{A6}), 8.48 (m, 1H, H^{C2}), 8.47 (s, 2H, H^{B3}), 8.42 (d, J = 7.8 Hz, 1H, H^{C6}), 7.89 (d, J = 7.8 Hz, 1H, H^{C4}), 7.82 (t, J = 7.8 Hz, 1H, H^{C5}), 7.59 (m, 2H, H^{A5}). $^{13}C\{^1H\}$ NMR (126 MHz, DMSO-d6): δ/ppm 154.8 (C^{B2}), 150.2 (C^{A6}), 148.4 (overlapping C^{A2+B4}), 138.3 (C^{C1}), 134.5 (C^{A4}), 133.8 (C^{A3}), 131.7 (C^{C6}), 130.1 (C^{C5}), 130.0 (q, J_{CF} = 31 Hz, C^{C3}), 126.0 (q, J_{CF} = 4 Hz, C^{C4}), 124.3 (q, J_{CF} = 4 Hz, C^{C2}), 124.1 (q, J_{CF} = 272 Hz, C^a), 123.8 (C^{A5}), 117.8 (C^{B3}). $^{19}F\{^1H\}$ NMR (565 MHz, DMSO-d6): δ/ppm −60.7. UV-VIS (MeCN, 2.0 × 10^{-5} mol dm^{-3}) λ/nm 248 (ε/dm^{-3} mol^{-1} cm^{-1} 40,870), 296 (6350). MALDI-TOF-MS *m/z* 378.10 $[M+H]^+$ (*calc.* 378.12). Found C 69.81, H 3.71, N 11.31; required for $C_{22}H_{14}F_3N_3$ C 70.02, H 3.74, N 11.14. See Figure S8 for the IR spectrum of **4**.

3.6. $[Cu_2(hfacac)_4(1)_2]_n \cdot 2nC_6H_4Cl_2$

A 1,2-dichlorobenzene (5 mL) solution of $[Cu(hfacac)_2]\cdot H_2O$ (29.7 mg, 0.060 mmol) was layered over a $CHCl_3$ solution (4 mL) of ligand **1** (11.3 mg, 0.030 mmol). Green block-like crystals grew after 1 day. A single crystal was selected for X-ray diffraction. The remaining crystals were washed with chloroform and 1,2-dichlorobenzene and analyzed by PXRD and IR spectroscopy.

For a preparative scale reaction, **1** (28.7 mg, 0.076 mmol) was dissolved in $CHCl_3$ (4 mL). Then a solution of $[Cu(hfacac)_2]\cdot H_2O$ (37.7 mg, 0.076 mmol) in 1,2-dichlorobenzene (5 mL) was added, and the green solution was stirred at room temperature. Immediate formation of a pale green precipitate was observed and stirring of the suspension at room temperature was continued for 44 h. The suspension was then centrifuged, the solid collected and dried in vacuo. $[Cu_2(hfacac)_4(\mathbf{1})_2]_n \cdot nC_6H_4Cl_2$ (64.4 mg, 0.035 mmol, 91.2%) was isolated as a pale green powder. Elemental analysis: found C 45.34, H 2.24, N 4.24;

required for $C_{70}H_{36}Cl_2Cu_2F_{30}N_6O_8$ C 45.27, H 1.95, N 4.53. PXRD analysis was performed (see text).

3.7. [Cu(hfacac)$_2$(2)]$_n$·2nC_6H_5Me

A toluene (5 mL) solution of [Cu(hfacac)$_2$]·H_2O (29.7 mg, 0.060 mmol) was layered over a $CHCl_3$ solution (4 mL) of compound **2** (11.3 mg, 0.030 mmol). Blue plate-like crystals grew after 4 days, and one X-ray quality crystal was chosen. The remaining crystals were washed with $CHCl_3$ and toluene and this bulk sample was analyzed by IR spectroscopy and PXRD.

A preparative scale reaction was also carried out. Ligand **2** (28.7 mg, 0.076 mmol) was dissolved in $CHCl_3$ (4 mL), and then a solution of [Cu(hfacac)$_2$]·H_2O (37.7 mg, 0.076 mmol) in toluene (5 mL) was added. The green solution was stirred at room temperature and immediate formation of a pale green precipitate was observed. After 44 h, the precipitate that formed was collected by centrifugation and dried *in vacuo*. [Cu(hfacac)$_2$(**2**)]$_n$ (43.7 mg, 0.051 mmol, 67.1%) was isolated as a pale green powder. Elemental analysis: found C 44.92, H 2.23, N 5.17; required for $C_{32}H_{16}CuF_{15}N_3O_4$ C 44.95, H 1.89, N 4.91. PXRD analysis was performed (see text).

3.8. [Cu$_2$(hfacac)$_4$(3)$_2$]$_n$·n$C_6H_4Cl_2$

A solution of [Cu(hfacac)$_2$]·H_2O (29.7 mg, 0.060 mmol) in 1,2-dichlorobenzene (5 mL) was layered over a $CHCl_3$ solution (4 mL) of compound **3** (11.3 mg, 0.030 mmol). Green plate-like crystals grew after 11 days. An X-ray quality single crystal was selected and the residual crystals were washed with $CHCl_3$ and 1,2-dichlorobenzene and analyzed by PXRD and IR spectroscopy.

On a preparative scale, compound **3** (28.7 mg, 0.076 mmol) was dissolved in chloroform (4 mL), and then a solution of [Cu(hfacac)$_2$]·H_2O (37.7 mg, 0.076 mmol) in 1,2-dichlorobenzene (5 mL) was added. The green solution was stirred at room temperature and the formation of a pale green precipitate was immediately observed. After 44 h, the suspension was then centrifuged, and the solid was collected and dried *in vacuo*. [Cu(hfac)$_2$(**3**)]$_n$ (57.4mg, 0.034 mmol, 88.3%) was isolated as a pale green powder. Elemental analysis: found C 45.13, H 2.08, N 4.83; required for $C_{32}H_{16}CuF_{15}N_3O_4$ C 44.95, H 1.89, N 4.91. PXRD analysis was performed (see text).

3.9. [Cu$_2$(hfacac)$_4$(3)$_2$]$_n$·nC_6H_5Cl

A solution of [Cu(hfacac)$_2$]·H_2O (29.7 mg, 0.060 mmol) in chlorobenzene (5 mL) was layered over a $CHCl_3$ solution (4 mL) of ligand **3** (11.3 mg, 0.030 mmol). Green plate-like crystals grew after 11 days. Single-crystal X-ray crystallography confirmed that the structure of [Cu$_2$(hfacac)$_4$(**3**)$_2$]$_n$·nC_6H_5Cl was essentially isostructural with [Cu$_2$(hfacac)$_4$(**3**)$_2$]$_n$·n $C_6H_4Cl_2$, and no bulk sample characterization was carried out.

3.10. [Cu(hfacac)$_2$(4)]$_n$·nC_6H_5Cl

A chlorobenzene (5 mL) solution of [Cu(hfacac)$_2$]·H_2O (29.7 mg, 0.060 mmol) was layered over a $CHCl_3$ solution (4 mL) of **4** (11.3 mg, 0.030 mmol). Green block-like crystals grew after 10 days. After the selection of a single crystal, the residual crystals were washed with $CHCl_3$ and chlorobenzene and this bulk sample was analyzed by PXRD and IR spectroscopy.

On a preparative scale, compound **4** (28.7 mg, 0.076 mmol) was dissolved in $CHCl_3$ (4 mL). Then a solution of [Cu(hfacac)$_2$]·H_2O (37.7 mg, 0.076 mmol) in chlorobenzene (5 mL) was added, and the green solution was stirred at room temperature. Immediate formation of a pale green precipitate was observed. After 44 h, the formed precipitate was collected by centrifugation and dried *in vacuo*. [Cu(hfacac)$_2$(**4**)]$_n$ (49.1 mg, 0.057 mmol, 75.0%) was obtained as a pale green powder. Elemental analysis: found C 44.78, H 2.03, N 5.22; required for $C_{32}H_{16}CuF_{15}N_3O_4$ C 44.95, H 1.89, N 4.91. PXRD analysis was performed (see text).

3.11. Crystallography

Single crystal data were collected either on a STOE StadiVari diffractometer (STOE & Cie GmbH, 64295 Darmstadt, Germany) equipped with a Metaljet D2 source (GaKα radiation) and a Pilatus300K detector, or on a Bruker APEX-II diffractometer (Bruker BioSpin AG, 8117 Fällanden, Switzerland) with CuKα radiation. For the former, data processing used STOE software (X-Area 1.90, STOE, 2020), and structures were solved using Superflip [50,51] and Olex2 [52], and the model was refined with ShelXL v. 2014/7 [53]. For the latter, data reduction, solution, and refinement used the programs APEX [54], ShelXT [55], Olex2 [52], and ShelXL v. 2014/7 [53]. All H atoms were included at geometrically calculated positions and refined using a riding model with U_{iso} = 1.2 of the parent atom. Structure analysis used CSD Mercury 2020.1 [56]. In the four coordination polymers, some CF_3 groups were disordered and these F atoms were refined isotropically. In [Cu2(hfacac)4(**1**)2]*n*·2*n*C6H4Cl2, one CF_3 group on each $[hfacac]^-$ ligand was rotationally disordered and was modeled over three positions with 0.5, 0.3 and 0.2 fractional occupancies for one CF_2 group, and 0.4, 0.4 and 0.2 fractional occupancies for the second. In $[Cu(hfacac)_2(\mathbf{2})]_n \cdot 2nC_6H_5Me$, one CF_3 group of an $[hfacac]^-$ ligand was disordered and was modeled over two positions with fractional occupancies of 0.6 and 0.4; one toluene molecule was also disordered, and the methyl group was modeled over two sites of equal occupancies. In $[Cu_2(\mathbf{3})_2(hfacac)_4]_n \cdot nC_6H_4Cl_2$, one $[hfacac]^-$ ligand contains one rotationally disordered CF_3 which was modeled over two equal occupancy sites; the CF_3 group in **3** was also disordered, and again was modeled over two sites with fractional occupancies of 0.5. In $[Cu_2(hfacac)_4(\mathbf{4})]_n \cdot nC_6H_5Cl$, the asymmetric unit contains half of one molecule of **4**, and the CF_3 group is disordered over two sites related by a mirror, and the whole group was refined isotropically; additionally, the CF_3 is rotationally disordered and was modeled over sites of fractional occupancies 0.3 and 0.2. A mask was used to treat the solvent region in $[Cu_2(hfacac)_4(\mathbf{4})]_n \cdot nC_6H_5Cl$ and the electron density removed equated to one C_6H_5Cl molecule per 2 Cu atoms; this was added to the formulae and appropriate numbers. In the structural discussions, only the major (or one of the equal) occupancy sites are considered in each disordered entity.

PXRD data were collected at room temperature in transmission mode using a Stoe Stadi P diffractometer (STOE & Cie GmbH, 64295 Darmstadt, Germany), equipped with CuKα1 radiation (Ge(111) monochromator and a DECTRIS MYTHEN 1K detector. Whole-pattern decomposition (profile matching) analysis [57–59] of the diffraction patterns was done using the package FULLPROF SUITE (v. September 2020) [59,60] using a previously determined instrument resolution function based on a NIST640d standard. The structural models were derived from the single crystal X-ray diffraction data. Refined parameters in Rietveld were scale factor, zero shift, lattice parameters, Cu and halogen atomic positions, background points, and peaks shapes as a Thompson-Cox-Hastings pseudo-Voigt function. Preferred orientations as a March–Dollase multi-axial phenomenological model were incorporated into the analysis.

1: $C_{22}H_{14}F_3N_3$, M_r = 377.36, colorless plate, monoclinic, space group $P2_1/c$, a = 10.5418(13), b = 21.653(3), c = 7.4248(9) Å, β = 94.146(4)°, V = 1690.3(4) Å^3, T = 150 K, Z = 4, $\mu(CuK_\alpha)$ = 0.947. Total 22080 reflections, 3110 unique (R_{int} = 0.0257). Refinement of 3056 reflections (253 parameters) with $I > 2\sigma(I)$ converged at final R_1 = 0.0347 (R_1 all data = 0.0350), wR_2 = 0.0916 ($wR2$ all data = 0.0919), F(000) = 776, gof = 1.028. CCDC 2077591.

2: $C_{22}H_{14}F_3N_3$, M_r = 377.36, colorless plate, triclinic, space group P–1, a = 7.5432(5), b = 10.8309(8), c = 21.3995(15) Å, α = 91.518(3), β = 98.791(2), γ = 98.418(2)°, V = 1707.0(2) Å^3, T = 150 K, Z = 4, $\mu(CuK_\alpha)$ = 0.937. Total 16588 reflections, 5996 unique (R_{int} = 0.0235). Refinement of 5541 reflections (505 parameters) with $I > 2\sigma(I)$ converged at final R_1 = 0.1767 (R_1 all data = 0.1784), wR_2 = 0.0601 ($wR2$ all data = 0.0629), F(000) = 776, gof = 1.109. CCDC 2077593.

$[Cu_2(hfacac)_4(\mathbf{1})_2]_n \cdot 2nC_6H_4Cl_2$: $C_{76}H_{40}Cl_4Cu_2F_{30}N_6O_8$, M_r = 2004.02, green block, orthorhombic, space group *Pbca*, a = 22.4688(13), b = 14.3450(8), c = 24.8918(14) Å, V = 8023.0(8) Å^3, T = 150 K, Z = 4, $\mu(CuK\alpha)$ = 3.050. Total 65061 reflections, 7433 unique (R_{int} = 0.0438).

Refinement of 6996 reflections (570 parameters) with $I > 2\sigma(I)$ converged at final $R_1 = 0.1509$ (R_1 all data = 0.1534), $wR_2 = 0.0589$ ($wR2$ all data = 0.0616), F(000) = 3992, gof = 1.029. CCDC 2077592.

$[Cu_2(hfacac)_4(\mathbf{2})]_n \cdot 2nC_6H_5Me$: $C_{46}H_{32}CuF_{15}N_3O_4$, $M_r = 1039.28$, blue plate, monoclinic, space group Cc, $a = 8.8604(2)$, $b = 25.3335(7)$, $c = 20.7490(6)$ Å, $\beta = 97.537(2)^\circ$, $V = 4617.2(2)$ Å^3, $T = 150$ K, $Z = 4$, $\mu(GaK_\alpha) = 3.168$. Total 13164 reflections, 5535 unique ($R_{int} = 0.0508$). Refinement of 5261 reflections (575 parameters) with $I > 2\sigma(I)$ converged at final $R_1 = 0.0802$ (R_1 all data = 0.0832), $wR_2 = 0.2115$ ($wR2$ all data = 0.2173), F(000) = 2100, gof = 1.019. CCDC 2077595.

$[Cu_2(hfacac)_4(\mathbf{3})_2]_n \cdot nC_6H_4Cl_2$: $C_{70}H_{36}Cl_2Cu_2F_{30}N_6O_8$, $M_r = 1857.03$, green plate, triclinic, space group P–1, $a = 11.9939(3)$, $b = 12.1658(3)$, $c = 12.9674(3)$ Å, $\alpha = 102.257(2)$, $\beta = 103.145(2)$, $\gamma = 91.214(2)^\circ$, $V = 1795.76(8)$ Å^3, $T = 150$ K, $Z = 1$, $\mu(GaK_\alpha) = 4.466$. Total 40977 reflections, 7061 unique ($R_{int} = 0.0352$). Refinement of 6430 reflections (510 parameters) with $I > 2\sigma(I)$ converged at final $R_1 = 0.0829$ (R_1 all data = 0.0884), $wR_2 = 0.2286$ ($wR2$ all data = 0.2355), F(000) = 924, gof = 1.068. CCDC 2077596.

$[Cu_2(hfacac)_4(\mathbf{3})_2]_n \cdot nC_6H_5Cl$: $C_{70}H_{37}ClCu_2F_{30}N_6O_8$, $M_r = 1822.58$, green plate, triclinic, space group P–1, $a = 11.9906(3)$, $b = 11.9911(3)$, $c = 13.0617(3)$ Å, $\alpha = 103.144(2)$, $\beta = 102.547(2)$, $\gamma = 91.491(2)^\circ$, $V = 1779.51(8)$ Å^3, $T = 150$ K, $Z = 1$, $\mu(GaK_\alpha) = 4.273$. Total 53503 reflections, 6936 unique ($R_{int} = 0.0598$). Refinement of 6607 reflections (510 parameters) with $I > 2\sigma(I)$ converged at final $R_1 = 0.0940$ (R_1 all data = 0.0965), $wR_2 = 0.2580$ ($wR2$ all data = 0.2613), F(000) = 908, gof = 1.090. CCDC 2077594.

$[Cu_2(hfacac)_4(\mathbf{4})]_n \cdot nC_6H_5Cl$: $C_{38}H_{21}ClCuF_{15}N_3O_4$, $M_r = 967.57$, green block, orthorhombic, space group $Pnma$, $a = 6.5155(4)$, $b = 26.2371(17)$, $c = 22.3188(15)$ Å, $V = 3815.4(4)$ Å^3, $T = 200.0$ K, $Z = 4$, $\mu(CuK_\alpha) = 0.845$. Total 24327 reflections, 3512 unique ($R_{int} = 0.0333$). Refinement of 3376 reflections (266 parameters) with $I > 2\sigma(I)$ converged at final $R_1 = 0.0640$ (R_1 all data = 0.0654), $wR_2 = 0.1707$ ($wR2$ all data = 0.1717), F(000) = 1932, gof = 1.128. CCDC 2077597.

4. Conclusions

We have prepared and characterized four new ligands **1**–**4** which comprise pairs with either 4,2′:6′,4″- or 3,2′:6′,3″-tpy metal-binding domains and with isomeric 4′-trifluoromethy lphenyl substituents. The single crystal structures of **1** and **2** were determined. Despite the change in the substitution position of the CF_3 group upon going from **1** to **2**, the packing interactions in the two compounds are similar and are dominated by face-to-face π-stacking, with the stacking interaction extending across the whole molecular framework. Reactions of **1**, **2**, **3** and **4** with $[Cu(hfacac)_2]\cdot H_2O$ under conditions of crystal growth by layering using a combination of $CHCl_3$ and an aromatic solvent resulted in the formation of $[Cu_2(hfacac)_4(\mathbf{1})_2]_n \cdot 2nC_6H_4Cl_2$, $[Cu(hfacac)_2(\mathbf{2})]_n \cdot 2nC_6H_5Me$, $[Cu_2(hfacac)_4(\mathbf{3})_2]_n \cdot nC_6H_4Cl_2$, $[Cu_2(hfacac)_4(\mathbf{3})_2]_n \cdot nC_6H_5Cl$, and $[Cu(hfacac)_2(\mathbf{4})]_n \cdot nC_6H_5Cl$. All are 1D-coordination polymers, and the two polymers containing **3** are essentially isostructural. PXRD analysis of the bulk crystalline products confirmed that the single crystals used for structure determination were representative of the bulk materials. PXRD was used to confirm that the same coordination compounds could be prepared on a preparative scale.

The 1D-polymers $[Cu_2(hfacac)_4(\mathbf{1})_2]_n \cdot 2nC_6H_4Cl_2$ and $[Cu(hfacac)_2(\mathbf{2})]_n \cdot 2nC_6H_5Me$ are zig-zag chains which follows from the V-shaped 4,2′:6′,4″-tpy building block. This structural motif is unaffected by changing the substitution position of the CF_3 group in **1** versus **2**. In both structures, packing interactions are dominated by C–F...F–C contacts, but the arrangement of the 1D-chains is significantly altered as a consequence of the directionalities of the C–CF_3 domains in **1** and **2**. There are no inter-polymer face-of-face π-stacking interactions, but instead, aromatic solvent molecules are incorporated into the lattice and engage in π-stacking contacts with the arene-backbone of both polymers.

In $[Cu_2(hfacac)_4(\mathbf{3})_2]_n \cdot nC_6H_4Cl_2$, the 3,2′:6′,3″-tpy adopts conformation **C** with an out/in arrangement of *N*-donors. A combination of this with Cu atoms on inversion centers

leads to an alternating arrangement of 3,2′:6′,3″-tpy units in the 1D-polymer. In contrast, the 3,2′:6′,3″-tpy unit in $[Cu(hfacac)_2(\mathbf{4})]_n \cdot n C_6H_5Cl$ exhibits conformation **A** (Scheme 1). The near coplanarity of the phenyl and central pyridine rings in **4** is notable and arises from the phenyl ring being locked in position by four $C–H_{phenyl}...F–C_{hfacac}$ contacts. In both $[Cu_2(hfacac)_4(\mathbf{3})_2]_n \cdot n C_6H_4Cl_2$ and $[Cu(hfacac)_2(\mathbf{4})]_n \cdot n C_6H_5Cl$, π-stacking interactions between 4′-trifluoromethylphenyl-3,2′:6′,3″-tpy domains are key packing interactions, and this contrasts with the packing of polymers incorporating **1** and **2**.

We have demonstrated that the assemblies of the coordination polymers in this work are reproducible, and that a switch from a 4,2′:6′,4″- to 3,2′:6′,3″-tpy metal-binding unit is accompanied by a change from dominant C–F...F–C and C–F...H–C contacts to π-stacking of arene domains between ligands **3** or **4**. The switch from a 3-CF_3 to 4-CF_3 substituent in the 4′-phenyl group has less significant consequences.

Supplementary Materials: The following are available online at https://www.mdpi.com/article/10.3390/inorganics9070054/s1, Figures S1–S4: Mass spectra of **1**–**4**; Figures S5–S8: IR spectra of **1**–**4**; Figure S9: Solution absorption spectra of **1**–**4**; Figures S10 and S11: ^1H and $^{13}C\{^1H\}$ NMR spectra of **1**–**4**; Figure S12: Packing of molecules of **2**; Figures S13–S16: Molecular structures of the asymmetric units in the coordination polymers; Figure S17: Packing in $[Cu(hfacac)_2(\mathbf{2})]_n \cdot 2n C_6H_5Me$; Figure S18: C–F...F–C and C–F...H–C contacts present in $[Cu_2(hfacac)_4(\mathbf{3})_2]_n \cdot n C_6H_4Cl_2$; Figure S19: Packing in $[Cu(hfacac)_2(\mathbf{4})]_n \cdot n C_6H_5Cl$; Figure S20–S23: IR spectra of the coordination polymers; Figures S24–S26: Additional PXRD data.

Author Contributions: G.M. and S.S.C. contributed equally to the research and writing. Project conceptualization, administration, supervision, and funding acquisition: C.E.H. and E.C.C.; investigation and data analysis: G.M. and S.S.C.; single-crystal X-ray diffraction and PXRD: A.P., G.M. and S.S.C.; manuscript writing: C.E.H., G.M. and S.S.C.; manuscript editing and review: all authors. All authors have read and agreed to the published version of the manuscript.

Funding: This research was funded in part by the Swiss National Science Foundation, grant number 200020_182559.

Data Availability Statement: The data presented in this study are available on request from the corresponding author. The data are not publicly accessible at present.

Acknowledgments: We thank the University of Basel for support of our research.

Conflicts of Interest: The authors declare no conflict of interest.

References

1. Housecroft, C.E. 4,2′:6′,4″-Terpyridines: Diverging and Diverse Building Blocks in Coordination Polymers and Metallomacrocycles. *Dalton Trans.* **2014**, *43*, 6594–6604. [CrossRef]
2. Housecroft, C.E. Divergent 4,2′:6′,4″- and 3,2′:6′,3″-Terpyridines as Linkers in 2- and 3-Dimensional Architectures. *CrystEngComm* **2015**, *17*, 7461–7468. [CrossRef]
3. Housecroft, C.E.; Constable, E.C. Ditopic and tetratopic 4,2′:6′,4″-Terpyridines as Structural Motifs in 2D- and 3D-Coordination Assemblies. *Chimia* **2019**, *73*, 462–467. [CrossRef]
4. Housecroft, C.E.; Constable, E.C. The Terpyridine Isomer Game: From Chelate to Coordination Network Building Block. *Chem. Commun.* **2020**, *56*, 10786–10794. [CrossRef] [PubMed]
5. Elahi, S.M.; Raizada, M.; Sahu, P.K.; Konar, S. Terpyridine-Based 3D Metal–Organic-Frameworks: A Structure–Property Correlation. *Chem. Eur. J.* **2021**, *27*, 5858–5870. [CrossRef] [PubMed]
6. Housecroft, C.E.; Constable, E.C. Isomers of terpyridine as ligands in coordination polymers and networks containing zinc(II) and cadmium(II). *Molecules* **2021**, *26*, 3110. [CrossRef]
7. Liu, B.; Hou, L.; Wu, W.-P.; Dou, A.-N.; Wang, Y.-Y. Highly selective luminescence sensing for Cu^{2+} ions and selective CO_2 capture in a doubly interpenetrated MOF with Lewis basic pyridyl sites. *Dalton Trans.* **2015**, *44*, 4423–4427. [CrossRef]
8. Wu, Y.; Wu, J.; Luo, Z.; Wang, J.; Li, Y.; Han, Y.; Liu, J. Fluorescence detection of Mn^{2+}, $Cr_2O_7^{2-}$ and nitroexplosives and photocatalytic degradation of methyl violet and rhodamine B based on two stable metal–organic frameworks. *RSC Adv.* **2017**, *7*, 10415–10423. [CrossRef]
9. Yuan, F.; Yuan, C.-M.; Hu, H.-M.; Wang, T.-T.; Zhou, C.-S. Structural diversity of a series of terpyridyl carboxylate coordination polymers: Luminescent sensor and magnetic properties. *J. Solid State Chem.* **2018**, *258*, 588–601. [CrossRef]

10. Dorofeeva, V.N.; Mishura, A.M.; Lytvynenko, A.S.; Grabovaya, N.V.; Kiskin, M.A.; Kolotilov, S.V.; Eremenko, I.L.; Novotortsev, V.M. Structure and Electrochemical Properties of Copper(II) Coordination Polymers with Ligands Containing Naphthyl and Anthracyl Fragments. *Theor. Exper. Chem.* **2016**, *52*, 111–118. [CrossRef]
11. Nijs, T.; Klein, Y.M.; Mousavi, S.F.; Ahsan, A.; Nowakowska, S.; Constable, E.C.; Housecroft, C.E.; Jung, T.A. The Different Faces of 4′-Pyrimidinyl-Functionalized 4,2′:6′,4′′-Terpyridines: Metal–Organic Assemblies from Solution and on Au(111) and Cu(111) Surface Platforms. *J. Am. Chem. Soc.* **2018**, *140*, 2933–2939. [CrossRef] [PubMed]
12. Constable, E.C.; Housecroft, C.E.; Vujovic, S.; Zampese, J.A.; Crochet, A.; Batten, S.R. Do perfluoroarene$\cdots$arene and C–H$\cdots$F interactions make a difference to the structures of 4,2′:6′,4′′-terpyridine-based coordination polymers? *CrystEngComm* **2013**, *15*, 10068–10078. [CrossRef]
13. Li, L.; Zhang, Y.Z.; Yang, C.; Liu, E.; Golen, J.A.; Zhang, G. One-dimensional copper(II) coordination polymers built on 4′-substituted 4,2′:6′,4′′- and 3,2′:6′,3′′-terpyridines: Syntheses, structures and catalytic properties. *Polyhedron* **2016**, *105*, 115–122. [CrossRef]
14. Constable, E.C.; Housecroft, C.E.; Neuburger, M.; Vujovic, S.; Zampese, J.A. Molecular recognition between 4′-(4-biphenylyl)-4,2′:6′,4′′-terpyridine domains in the assembly of d^9 and d^{10} metal ion-containing one-dimensional coordination polymers. *Polyhedron* **2013**, *60*, 120–129. [CrossRef]
15. Rocco, D.; Novak, S.; Prescimone, A.; Constable, E.C.; Housecroft, C.E. Manipulating the conformation of 3,2′:6′,3′′-terpyridine in $[Cu_2(\mu\text{-}OAc)_4(3,2'{:}6',3''\text{-tpy})]_n$ 1D-polymers. *Chemistry* **2021**, *3*, 15. [CrossRef]
16. Rocco, D.; Manfroni, G.; Prescimone, A.; Klein, Y.M.; Gawryluk, D.J.; Constable, E.C.; Housecroft, C.E. Single and double-stranded 1D-coordination polymers with 4′-(4-alkyloxyphenyl)-3,2′:6′,3′′-terpyridines and $\{Cu_2(\mu\text{-}OAc)_4\}$ or $\{Cu_4(\mu_3\text{-}OH)_2(\mu\text{-}OAc)_2(\mu_3\text{-}OAc)_2(AcO\text{-}\kappa O)_2\}$ motifs. *Polymers* **2020**, *12*, 318. [CrossRef]
17. Klein, Y.M.; Prescimone, A.; Constable, E.C.; Housecroft, C.E. Coordination behaviour of 1-(4,2′:6′,4′′-terpyridin-4′-yl)ferrocene and 1-(3,2′:6′,3′′-terpyridin-4′-yl)ferrocene: Predictable and unpredictable assembly algorithms. *Aust. J. Chem.* **2017**, *70*, 468–477. [CrossRef]
18. Khatua, S.; Goswami, S.; Biswas, S.; Tomar, K.; Jena, H.S.; Konar, S. Stable Multiresponsive Luminescent MOF for Colorimetric Detection of Small Molecules in Selective and Reversible Manner. *Chem. Mater.* **2015**, *27*, 5349–5360. [CrossRef]
19. Khatua, S.; Biswas, P. Flexible Luminescent MOF: Trapping of Less Stable Conformation of Rotational Isomers, In Situ Guest-Responsive Turn-Off and Turn-On Luminescence and Mechanistic Study. *ACS Appl. Mater. Interfaces* **2020**, *12*, 22335–22346. [CrossRef]
20. Khatua, S.; Bar, A.K.; Konar, S. Tuning Proton Conductivity by Interstitial Guest Change in Size-Adjustable Nanopores of a Cu^I-MOF: A Potential Platform for Versatile Proton Carriers. *Chem. Eur. J.* **2016**, *22*, 16277–16285. [CrossRef]
21. Li, X.-Z.; Zhou, X.-P.; Li, D.; Yin, Y.-G. Controlling interpenetration in CuCN coordination polymers by size of the pendant substituents of terpyridine ligands. *CrystEngComm* **2011**, *13*, 6759–6765. [CrossRef]
22. Xi, Y.; Wei, W.; Xu, Y.; Huang, X.; Zhang, F.; Hu, C. Coordination Polymers Based on Substituted Terpyridine Ligands: Synthesis, Structural Diversity, and Highly Efficient and Selective Catalytic Oxidation of Benzylic C–H Bonds. *Cryst. Growth Des.* **2015**, *15*, 2695–2702. [CrossRef]
23. Liu, C.; Ding, Y.-B.; Shi, X.-H.; Zhang, D.; Hu, M.-H.; Yin, Y.-G.; Li, D. Interpenetrating Metal−Organic Frameworks Assembled from Polypyridine Ligands and Cyanocuprate Catenations. *Cryst. Growth Des.* **2009**, *9*, 1275–1277. [CrossRef]
24. Wang, J.; Yuan, F.; Hu, H.-M.; Bai, C.; Xue, G.-L. Nitro explosive and cation sensing by a luminescent 2D Cu(I) coordination polymer with multiple Lewis basic sites. *Inorg. Chem. Commun.* **2016**, *73*, 37–40. [CrossRef]
25. Klein, Y.M.; Lanzilotto, A.; Prescimone, A.; Krämer, K.W.; Decurtins, S.; Liu, S.-X.; Constable, E.C.; Housecroft, C.E. Coordination behaviour of 1-(3,2′:6′,3′′-terpyridin-4′-yl)ferrocene: Structure and magnetic and electrochemical properties of a tetracopper dimetallomacrocycle. *Polyhedron* **2017**, *129*, 71–76. [CrossRef]
26. Yuan, F.; Xie, J.; Hu, H.-M.; Yuan, C.-M.; Xu, B.; Yang, M.-L.; Dong, F.-X.; Xue, G.-L. Effect of pH/metal ion on the structure of metal–organic frameworks based on novel bifunctionalized ligand 4′-carboxy-4,2′:6′,4′′-terpyridine. *CrystEngComm* **2013**, *15*, 1460–1467. [CrossRef]
27. Gong, Y.; Zhang, M.M.; Zhang, P.; Shi, H.F.; Jiang, P.G.; Lin, J.H. Metal–organic frameworks based on 4-(4-carboxyphenyl)-2,2,4,4-terpyridine: Structures, topologies and electrocatalytic behaviors in sodium laurylsulfonate aqueous solution. *CrystEngComm* **2014**, *16*, 9882–9890. [CrossRef]
28. Yang, W.; Lin, X.; Jia, J.; Blake, A.J.; Wilson, C.; Hubberstey, P.; Champness, N.R.; Schröder, M. A biporous coordination framework with high H_2 storage density. *Chem. Commun.* **2008**, 359–361. [CrossRef]
29. Wu, Y.; Lu, L.; Feng, J.; Li, Y.; Sun, Y.; Ma, A. Design and construction of diverse structures of coordination polymers: Photocatalytic properties. *J. Solid State Chem.* **2017**, *245*, 213–218. [CrossRef]
30. Zhang, L.; Li, C.-J.; He, J.-E.; Chen, Y.-Y.; Zheng, S.-R.; Fan, J.; Zhang, W.-G. Construction of New Coordination Polymers from 4′-(2,4-disulfophenyl)- 3,2′:6′3′′-terpyridine: Polymorphism, pH-dependent syntheses, structures, and properties. *J. Solid State Chem.* **2016**, *233*, 444–454. [CrossRef]
31. Zhu, S.; Dai, X.-J.; Wang, X.-G.; Cao, Y.-Y.; Zhao, X.-J.; Yang, E.-C. Two Bulky Conjugated 4′-(4-Hydroxyphenyl)-4,2′:6′,4′′-terpyridine-based Layered Complexes: Synthesis, Structure, and Photocatalytic Hydrogen Evolution Activity. *Z. Anorg. Allg. Chem.* **2019**, *645*, 516–522. [CrossRef]

32. Zuo, T.; Luo, D.; Huang, Y.-L.; Li, Y.Y.; Zhou, X.-P.; Li, D. Chiral 3D coordination polymers consisting of achiral terpyridyl precursors: From spontaneous resolution to enantioenriched induction. *Chem. Eur. J.* **2020**, *26*, 1936–1940. [CrossRef]
33. Lusi, M.; Fechine, P.B.A.; Chen, K.-J.; Perry, J.J.; Zaworotko, M.J. A rare cationic building block that generates a new type of polyhedral network with "cross-linked" pto topology. *Chem. Commun.* **2016**, *52*, 4160–4162. [CrossRef] [PubMed]
34. Groom, C.R.; Bruno, I.J.; Lightfoot, M.P.; Ward, S.C. The Cambridge Structural Database. *Acta Cryst.* **2016**, *B72*, 171–179. [CrossRef] [PubMed]
35. Bruno, I.J.; Cole, J.C.; Edgington, P.R.; Kessler, M.; Macrae, C.F.; McCabe, P.; Pearson, J.; Taylor, R. New software for searching the Cambridge Structural Database and visualizing crystal structures. *Acta Cryst.* **2002**, *B58*, 389–397. [CrossRef]
36. Toledo, D.; Vega, A.; Pizarro, N.; Baggio, R.; Pena, O.; Roisnel, T.; Pivan, J.-Y.; Moreno, Y. Comparitive study on structural, magnetic and spectroscopic properties of four new copper(II) coordination polymers with 4′-substituted terpyridine ligands. *J. Solid State Chem.* **2017**, *253*, 78–88. [CrossRef]
37. Toledo, D.; Ahumada, G.; Manzur, C.; Roisnel, T.; Pena, O.; Hamon, J.-R.; Pivan, J.-Y.; Moreno, Y. Unusual trinuclear complex of copper(II) containing a 4′-(3-methyl-2-thienyl)-4,2′:6′,4″-terpyridine ligand. Structural, spectroscopic, electrochemical and magnetic properties. *J. Mol. Struct.* **2017**, *1146*, 213–221. [CrossRef]
38. Lopez-Periago, A.; Vallcorba, O.; Frontera, C.; Domingo, C.; Ayllón, J.A. Exploring a novel preparation method of 1D metal organic frameworks based on supercritical CO_2. *Dalton Trans.* **2015**, *44*, 7548–7553. [CrossRef]
39. Delgado, S.; Barrilero, A.; Molina-Ontoria, A.; Medina, M.-E.; Pastor, C.J.; Jiménez-Aparicio, R.; Priego, J.L. Novel Coordination Polymers Generated from Angular 2,2′-Dipyridyl Ligands and Bis(hexafluoroacetylacetonate) Copper(II): Crystal Structures and Magnetic Properties. *Eur. J. Inorg. Chem.* **2006**, 2746–2759. [CrossRef]
40. Winter, S.; Weber, E.; Eriksson, L.; Csoregh, I. New coordination polymer networks based on copper(ii) hexafluoroacetylacetonate and pyridine containing building blocks: Synthesis and structural study. *New J. Chem.* **2006**, *30*, 1808–1819. [CrossRef]
41. Wang, J.; Hanan, G.S. A facile route to sterically hindered and non-hindered 4′-aryl-2,2′:6′,2″-terpyridines. *Synlett* **2005**, *2005*, 1251–1254. [CrossRef]
42. Smith, R.M.; Martell, A.E. *Critical Stability Constants*; Plenum Press: New York, NY, USA, 1975; Volume 2.
43. Yi, H.; Albrecht, M.; Pan, F.; Valkonen, A.; Rissanen, K. Stacking of Sterically Congested Trifluoromethylated Aromatics in their Crystals—The Role of Weak F···π or F···F Contacts. *Eur. J. Org. Chem.* **2020**, 6073–6077. [CrossRef]
44. Bondi, A. van der Waals volumes and radii. *J. Phys. Chem.* **1964**, *68*, 441–451. [CrossRef]
45. Rowland, R.S.; Taylor, R. Intermolecular Nonbonded Contact Distances in Organic Crystal Structures: Comparison with Distances Expected from van der Waals Radii. *J. Phys. Chem.* **1996**, *100*, 7384–7391. [CrossRef]
46. Spilfogel, T.S.; Titi, H.M.; Friščić, T. Database Investigation of Halogen Bonding and Halogen...Halogen Interactions between Porphyrins: Emergence of Robust Supamolecular Motifs and Frameworks. *Cryst. Growth Des.* **2021**, *21*, 1810–1832. [CrossRef]
47. Levina, E.O.; Chernyshov, I.Y.; Voronin, A.P.; Alekseiko, L.N.; Stash, A.I.; Vener, M.V. Solving the enigma of weak fluorine contacts in the solid state: A periodic DFT study of fluorinated organic crystals. *RSC Adv.* **2019**, *9*, 12520–12537. [CrossRef]
48. Reichenbächer, K.; Süss, H.I.; Hulliger, J. Fluorine in crystal engineering—"The little atom that could". *Chem. Soc. Rev.* **2005**, *34*, 22–30. [CrossRef]
49. Nakamoto, K. *Infrared and Raman Spectra of Inorganic Compounds, Part B*, 6th ed.; Wiley: Hoboken, NJ, USA, 2009; p. 99.
50. Palatinus, L.; Chapuis, G. Superflip—A Computer Program for the Solution of Crystal Structures by Charge Flipping in Arbitrary Dimensions. *J. Appl. Cryst.* **2007**, *40*, 786–790. [CrossRef]
51. Palatinus, L.; Prathapa, S.J.; Van Smaalen, S. EDMA: A Computer Program for Topological Analysis of Discrete Electron Densities. *J. Appl. Cryst.* **2012**, *45*, 575–580. [CrossRef]
52. Dolomanov, O.V.; Bourhis, L.J.; Gildea, R.J.; Howard, J.A.K.; Puschmann, H. Olex2: A Complete Structure Solution, Refinement and Analysis Program. *J. Appl. Cryst.* **2009**, *42*, 339–341. [CrossRef]
53. Sheldrick, G.M. Crystal Structure Refinement with ShelXL. *Acta Cryst.* **2015**, *C27*, 3–8. [CrossRef]
54. *Software for the Integration of CCD Detector System Bruker Analytical X-Ray Systems*; Bruker axs: Madison, WI, USA, 2001.
55. Sheldrick, G.M. ShelXT-Integrated space-group and crystal-structure determination. *Acta Cryst.* **2015**, *A71*, 3–8. [CrossRef] [PubMed]
56. Macrae, C.F.; Sovago, I.; Cottrell, S.J.; Galek, P.T.A.; McCabe, P.; Pidcock, E.; Platings, M.; Shields, G.P.; Stevens, J.S.; Towler, M.; et al. Mercury 4.0: From visualization to analysis, design and prediction. *J. Appl. Cryst.* **2020**, *53*, 226–235. [CrossRef] [PubMed]
57. LeBail, A.; Duroy, H.; Fourquet, J.L. Ab-initio structure determination of $LiSbWO_6$ by X-ray powder diffraction. *Mat. Res. Bull.* **1988**, *23*, 447–452. [CrossRef]
58. Pawley, G.S. Unit-cell refinement from powder diffraction scans. *J. Appl. Cryst.* **1981**, *14*, 357–361. [CrossRef]
59. Rodríguez-Carvajal, J. Recent Advances in Magnetic Structure Determination by Neutron Powder Diffraction. *Physica B* **1993**, *192*, 55–69. [CrossRef]
60. Roisnel, T.; Rodríguez-Carvajal, J. WinPLOTR: A Windows tool for powder diffraction patterns analysis Materials Science Forum. In Proceedings of the Seventh European Powder Diffraction Conference (EPDIC 7), Barcelona, Spain, 20–23 May 2000; pp. 118–123.